INFORMATION TO USERS

This manuscript has been reproduced from the microfilm master. UMI films the text directly from the original or copy submitted. Thus, some thesis and dissertation copies are in typewriter face, while others may be from any type of computer printer.

The quality of this reproduction is dependent upon the quality of the copy submitted. Broken or indistinct print, colored or poor quality illustrations and photographs, print bleedthrough, substandard margins, and improper alignment can adversely affect reproduction.

In the unlikely event that the author did not send UMI a complete manuscript and there are missing pages, these will be noted. Also, if unauthorized copyright material had to be removed, a note will indicate the deletion.

Oversize materials (e.g., maps, drawings, charts) are reproduced by sectioning the original, beginning at the upper left-hand corner and continuing from left to right in equal sections with small overlaps.

Photographs included in the original manuscript have been reproduced xerographically in this copy. Higher quality 6" x 9" black and white photographic prints are available for any photographs or illustrations appearing in this copy for an additional charge. Contact UMI directly to order.

Bell & Howell Information and Learning
300 North Zeeb Road, Ann Arbor, MI 48106-1346 USA
800-521-0600

Production of a cooled ion beam by manipulation of 60-keV ions into a radio-frequency quadrupole ion guide

Alban Kellerbauer

Foster Radiation Laboratory
Department of Physics

McGill University, Montréal (Québec)

January 1999

A thesis submitted to the Faculty of Graduate Studies and Research in partial fulfilment of the requirements of the degree of Master of Science (M. Sc.)

Für meine Eltern

Table of contents

Abstract v

Résumé vi

Acknowledgements vii

1 Introduction 1

2 Motivation 4

2.1 The ISOLDE facility at CERN 4

2.2 The ISOLTRAP experiment 5

2.3 Review of decelerators at ISOLTRAP 8

3 Background 11

3.1 RF confinement 11

3.2 Buffer gas damping and diffusion 15

3.3 Phase space and Liouville's theorem 18

3.4 Phase space volume of an ion beam 20

3.5 Phase space volume of an RFQ trap 23

3.6 Twiss parameters 24

3.7 Design goals / requirements 25

4 Computer simulation 26

4.1 Simulations performed at McGill University 26

4.2 Simulations performed at CERN 34

5 Data and results 38

5.1 Apparatus 38

5.2 Measurements performed at CERN 41

5.3 Measurements performed at McGill University 44

6 Conclusion 50

References 51

Appendix A: Technical drawings 53

Appendix B: Photographs 60

Abstract

An electrostatic deceleration system was developed for the injection of the 60-keV mass-separated ion beam at the ISOLDE facility at CERN (Geneva, Switzerland) into a new segmented radio-frequency quadrupole (RFQ) ion guide at the ISOLTRAP experiment. A detailed computer simulation of the ion motion through the electrostatic decelerating and focusing electrodes into the RFQ ion guide was carried out. A complete decelerating structure was designed and built using the parameters extracted from the simulation, as was the first half of a segmented RFQ ion guide for capturing and cooling the decelerated beam. With experiments conducted partly with the ISOLTRAP apparatus at CERN and partly with our apparatus at McGill University, we were able to show that the decelerating structure can in fact inject a beam into the RFQ ion guide. The measured transmission rate of 15 to 30 percent is in agreement with the value that was predicted by the simulations.

Résumé

Un système électrostatique a été développé pour décélérer le faisceau d'ions d'une énergie de 60 keV de l'installation ISOLDE au CERN (Genève, Suisse) vers l'intérieur d'un nouveau guide d'ions segmenté à champ électrique quadrupolaire oscillant à hautes fréquences (guide d'ions RFQ) à l'expérience ISOLTRAP. Une simulation détaillée sur ordinateur a été menée sur le mouvement des ions se déplaçant à travers les électrodes de décélération à potentiels électrostatiques et des électrodes de focalisation jusqu'à l'intérieur du guide d'ions. Une structure de décélération complète ainsi que la première moitié d'un guide d'ions RFQ segmenté pour la capture et le refroidissement du faisceau décéléré ont été conçues et construites en utilisant les paramètres obtenus lors des simulations. À l'aide des expériences menées en partie avec l'installation ISOLTRAP au CERN et en partie avec notre installation à l'Université McGill, nous avons démontré que la structure décélératrice permet en effet d'injecter un faisceau dans un guide d'ions RFQ. Le taux de transmission de 15 à 30 pour cent qui a été mesuré est en accord avec celui suggéré par les simulations.

Acknowledgements

I want to thank my supervisor Prof. Robert B. Moore for his help and inspiration both with the experimental work and with this thesis, Peter Varfalvy for his work for the simulations as well as help with the experiment, and Leo Nikkinen for invaluable assistance with electronics. A large portion of the machining of the deceleration apparatus and the ion guide was done by the summer student Thomas Sallès. The summer student Anders Vang-Pedersen built most of the components of the ion source used in the experiment. Thanks also to Taeman Kim, Van Fong, and Ali Al-Alousi, my other colleagues in the Ion Manipulation Group, for their support and encouragement. During my stay at CERN in fall of 1998, I appreciated the support of Dr. Georg Bollen, Dr. Emily Lamour, Sylvain Henry, Jens Dilling, and Frank Herfurth.

I want to acknowledge the financial support by my supervisor, as well as the additional financial support by the CERN ISOLDE group during my stay at CERN.

Prof. Jean Barrette, then director of the Graduate Studies Committee of the Department of Physics, made it possible for me to begin my studies at McGill University shortly after I arrived in Montréal in fall of 1994. I thank him for the confidence he had in me.

1 Introduction

In modern science and technology, there is a rising demand for high-quality beams of exotic ions. The fields in which such demands are made range from biomedical research, where the ions of interest are those of rare bio-molecules such as drugs in blood, to nuclear physics where the ions of interest are those of very unstable radio-nuclides which can only be produced by large high-energy particle accelerators and then only in quantities measured in atoms per second.

The need for high quality in the beams of such ions arises from the difficulty of separating, identifying and studying them in the vast background of uninteresting ions of normal material with which they are almost always associated in their production processes. Essentially, the smaller the volume occupied by the ions and the smaller the range of their momenta, the easier it is to find them. In technical terms, the smaller the phase space volume (the six-dimensional volume of the points representing the ions in a space made up of the three position and the three momentum co-ordinates), the easier it is to study them. The quality of an ion beam can be expressed as the inverse of this phase space volume.

Unfortunately, because of the very small quantities of available material to start with, the production of ions of that material must be optimised with respect to achieving the highest ionisation efficiency, rather than the smallest possible phase space volume. And ion sources optimised for efficiency of ionisation of available material usually provide ions with a larger phase space volume than can be accommodated by the high-precision instruments that can separate, identify and study them.

There is therefore a need for mechanisms to condense the phase space volume of collections of ions without throwing any of them away. Such a process is called "cooling" and this thesis addresses the problem of cooling ion beams of very unstable radio-nuclides that are of interest in low energy nuclear physics. Such beams are usually available at energies of around 50 keV.

One of the most remarkable demonstrations of the benefits of beam cooling was that of stored antiproton beams at CERN in Geneva, Switzerland in the early 1980's [1]. Here, cooling was achieved by having an intense cold beam of electrons at the same velocity as the antiprotons ride alongside the antiprotons for a short length of their path. The antiprotons therefore see a surrounding cloud of apparently stationary cold electrons and come into thermal equilibrium with them through Coulomb interactions. This cooling allowed the very rare antiprotons produced by high-energy collisions to be accumulated into very concentrated phase space volumes in a storage ring and precisely manipulated to interact with protons. In this Nobel award work, the small phase space volumes in which the interactions were made to take place allowed the observation of the elusive intermediate vector bosons that the interactions produced. The significance of this work lies in the belief that these bosons were fundamental building blocks of the Universe in its very early stages after the Big Bang.

Recently, a similar electron cooling technique was used on very-high-energy ions of heavy radio-nuclides stored in the Experimental Storage Ring (ESR) at GSI in Darmstadt, Germany [1]. This rendered the stored ion beams into a small enough phase space volume to allow precise mass measurements on a large number of radio-nuclides that could play a significant role in the dynamics of exploding stars. These results are soon to be published.

While the work in high-energy particle physics clearly demonstrated the benefits of beam cooling, the techniques employed in that field are not applicable to the relatively low-energy beams of ions of the radio-nuclides of interest here. However, recent work by Taeman Kim [2] has demonstrated that cooling of such beams is possible using the very natural, and very rapid, cooling of ions that results from simply bathing them in a thin neutral background gas (often referred to as a "buffer gas"). Until that work, such an obvious cooling technique was inapplicable because of the diffusion of the ions throughout the gas after they were cooled. Thus while the momentum

aspect of the phase space volume is condensed, the spatial volume becomes unlimited. In the work of Kim, it was shown that it is possible to constrain the volume of the ions by a transverse radio-frequency quadrupole field that confines them radially while they are allowed to drift along the axis of the field to form a beam. A device that employs this technique is commonly called an "RFQ ion guide".

However, unlike the cooling of ion beams by a collinear electron beam where the ions retain their axial velocity, the cooling of ions by a buffer gas brings the ions to rest in all directions. To form them into a beam once again, they have to be dragged out of the buffer gas and re-accelerated. Furthermore, the original ion beam to which cooling would be a benefit is usually itself at high axial velocity, too high in fact to be brought to rest in a reasonable distance in a buffer gas. Application of buffer gas cooling to ion beams therefore requires consideration of the deceleration of the ions before they enter the gas and their acceleration out of the gas after they are cooled.

The acceleration of cooled ions out of an RFQ ion guide has been dealt with in the work of Kim, who demonstrated that 100-eV ions injected into an RFQ ion guide filled with buffer gas could be very efficiently captured, cooled to about room temperature and re-accelerated to high energy as a very high-quality beam. What remained to be achieved in order to adapt the technique to higher velocity beams was to decelerate the ions so that they can be captured and cooled in such an RFQ ion guide. The design, implementation and testing of a system that can accomplish this is the subject of this thesis.

2 Motivation

2.1 The ISOLDE facility at CERN

Proton synchrotron booster

The ISOLDE (Isotope Separator On-Line) facility at CERN was built to produce radioactive nuclides in spallation, fission, or fragmentation reactions [3]. Since 1992, it is using a 1-GeV proton beam from the Proton Synchrotron Booster (PSB). The PSB is a stack of four small synchrotrons that pre-accelerate protons before injecting them into the Proton Synchrotron (PS), which in turn supplies all of CERN's high energy accelerators. About half of the pulses from the PSB are available for the bombardment of the ISOLDE target. The ISOLDE experiment hall is situated about 100 m from the PS Booster, at CERN's Meyrin site.

Targets and separators

The protons from the PSB are delivered to one of the two ISOLDE target zones and their corresponding different isotope separators. From either of those separators, the beam can be distributed to any of the experiments in the experiment hall.

The radioactive nuclides produced from a thick target placed in the PSB beam are ionised, accelerated to 60 keV, and mass-analysed. The two separators GPS (General Purpose Separator) and HRS (High Resolution Separator) have resolving powers of $M/\Delta M = 2400$ and $M/\Delta M = 10{,}000$, respectively.

Targets can consist of molten metals that are kept at temperatures of up to 1400 °C, or of refractory metal powder or fibrous carbides at temperatures above 2000 °C. The development of targets is a field of radiochemistry which requires knowledge and experience in many other fields of physics and chemistry. New target techniques and materials are constantly being investigated.

Physics programme

The ISOLDE facility is of interest for a great variety of disciplines. Experiments range from nuclear and atomic physics to nuclear solid state physics, nuclear astrophysics, biophysics, and nuclear medicine. Because ISOLDE offers the possibility to study the nuclear properties over a very wide range of elements and isotopes, the installation is of particular interest to nuclear physicists. One of the activities being carried out in this area is the ISOLTRAP experiment.

2.2 The ISOLTRAP experiment

Overview of the set-up of the facility

ISOLTRAP is an experiment for high-precision nuclear mass measurements [4]. With this spectrometer, the masses of more than 100 radioactive nuclei have so far been measured.

Figure 1 shows the three electromagnetic traps that make up the ISOLTRAP facility. Their respective functions are briefly described in the following paragraphs.

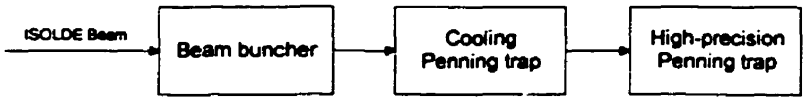

Figure 1: Schematic of the complete ISOLTRAP facility.

The tandem Penning trap system

The ISOLTRAP mass measurement set-up consists of two Penning traps ("tandem Penning trap system"). The first one is a cooling Penning trap, the second one the actual mass spectrometer.

Figure 2 shows the spatial arrangement of the two Penning traps. In 1996, the cooling and bunching trap shown in Fig. 2 was replaced with a gas-filled cylindrical Penning trap [5]. This new Penning trap is located in the homogeneous field of a 4.7-T super-conducting magnet. Its installation has led

to an increase of the capture efficiencies, and it has a sufficient mass resolving power to separate isobars.

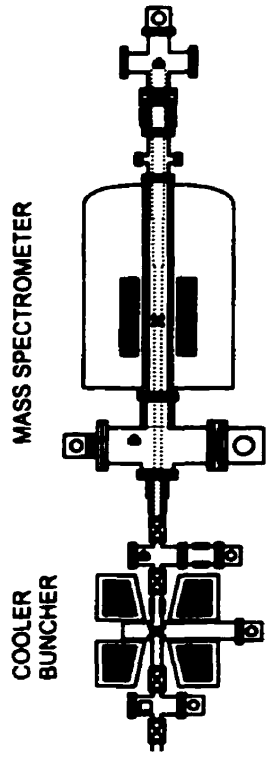

Figure 2: Layout of the experimental set-up of the ISOLTRAP tandem Penning trap system in 1996 (from [4]).

Mass measurement

In the ISOLTRAP high-precision Penning trap, the masses of ions are measured by determining their cyclotron frequency. The motion of an ion in an ideal Penning trap is the superposition of three independent harmonic motions [4]. These motions are shown schematically in Fig. 3. The axial harmonic motion is an oscillation with the frequency

$$\omega_z = \sqrt{\frac{qU_0}{md^2}}. \qquad (1)$$

The two radial motions have the frequencies

$$\omega_\pm = \frac{\omega_c}{2} \pm \sqrt{\frac{\omega_c^2}{4} - \frac{\omega_z^2}{2}}. \qquad (2)$$

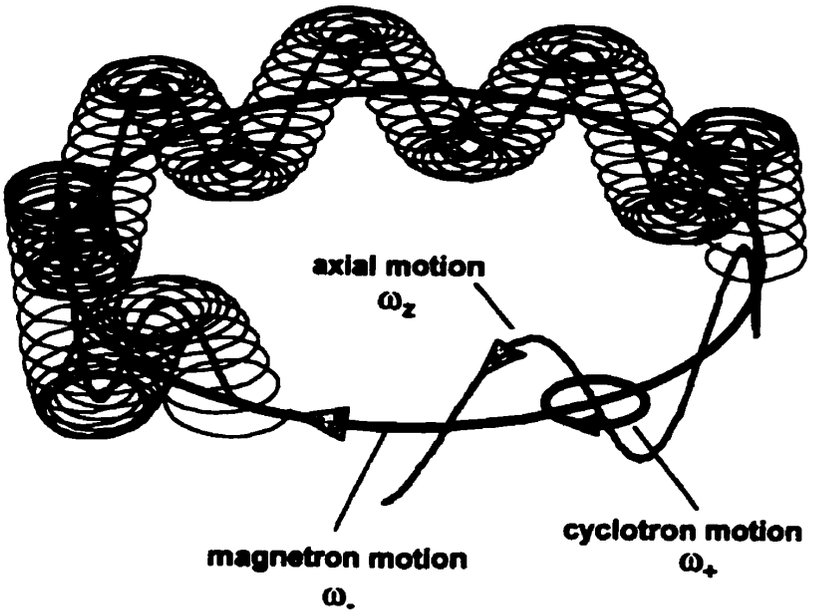

Figure 3: The three eigen-motions of an ion in an ideal Penning trap (from [4]).

The sum of both radial frequencies is the cyclotron frequency of an ion in a pure magnetic field:

$$\omega_c = \omega_+ + \omega_- , \tag{3}$$

which is a simple function of the mass and charge of the particles and of the amplitude of the magnetic field in which they oscillate:

$$\omega_c = \frac{q}{m} B . \tag{4}$$

In reality, many deviations from this idealisation must be corrected for. Those deviations can be electric or magnetic field imperfections, or a misalignment of the fields relative to each other.

Driving fields are used to excite the motions of the ions in the trap. By carefully choosing the frequency of the driving field, unwanted species in the trap can be removed. Their cyclotron amplitude simply increases until they leave the containment region. A driving field with the cyclotron frequency has the effect of coupling the two radial motions of the particles and of converting the particle oscillation to pure cyclotron motion. The particles gain kinetic energy in the process. The ions are ejected out of the trap and they drift

through an inhomogeneous magnetic field towards an ion detector. The magnetic field is designed so that particles that have gained more kinetic energy from the conversion of their radial motion also gain more axial energy in the magnetic field and thus reach the detector earlier. The time of flight to the detector is therefore lowest when the driving frequency is exactly equal to the cyclotron frequency of the ions. If the amplitude of the magnetic field is known to high accuracy, the mass of the particle can then be calculated from Eq. (4).

Collection and deceleration system

The ISOLTRAP project can be divided into two distinct tasks: The development of a high-precision Penning trap mass measurement system and the development of a collection and cooling system which can deliver a continuous radioactive beam to the measuring apparatus. The ISOLDE beam is highly radioactive and often dirty, and the Penning mass measurement trap requires very cool and very pure bunches of ions at repetition rates of about 1 Hz. The greatest challenge to the ISOLTRAP project has been the development of an efficient deceleration and beam preparation system that meets those requirements.

2.3 Review of decelerators at ISOLTRAP

The surface ionisation collection system

In its original configuration, the cooling Penning trap also served as the deceleration device for the 60-keV ion beam [4]. At is entrance, the ISOLDE beam was deposited on a rhenium foil for a period of time. The foil was then turned around by 180° and heated so that the radioactive ions were surface-ionised and released from the surface of the foil into the trap.

This system, while workable, was very inefficient and led to problems of contamination associated with having the heated foil so close to the collection Penning trap. With the development of the larger Penning trap collector described above, the implantation foil could be moved outside the region of

the Penning trap and the problems of contamination were considerably reduced. However, the technique was still restricted to only those elements that could be surface ionised by a hot foil. These are the alkali metals and the alkali earths.

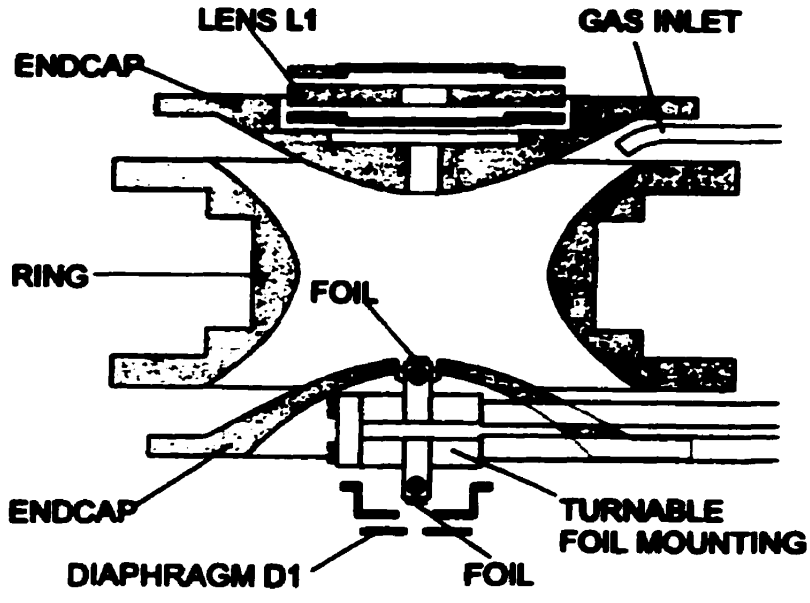

Figure 4: Low-precision Penning trap and foil collection system in the original ISOLTRAP configuration (from [4]).

The Paul trap collection and buncher system

The restriction imposed by ionisation by a heated foil was removed by the introduction of a Paul trap as a collector [6]. Here the incoming 60-keV ion beam was decelerated electrostatically to low energies, very much as in the work of this thesis. However, the decelerated beam was injected directly into a very large Paul trap.

It was hoped that just from the volume of the trap, a sufficient proportion of the incoming ions would be captured and delivered to the tandem Penning trap system. This was indeed the case, and it became possible to carry out experiments on radio-nuclides, such as those of mercury, that had previously been impossible with the heated-foil technique. However, the efficiencies were

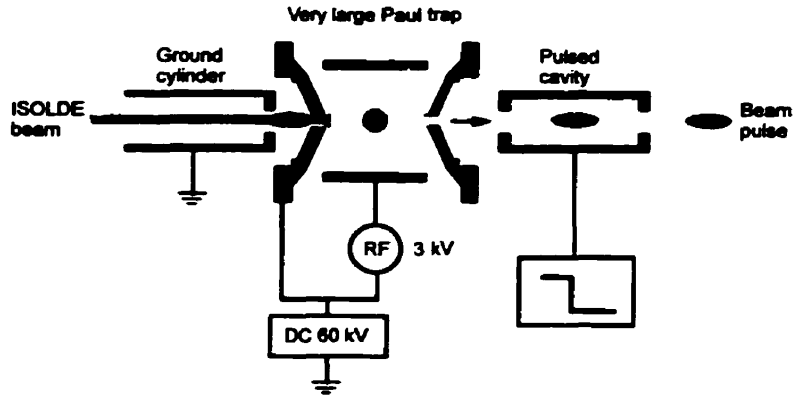

Figure 5: The very large Paul trap collection and buncher system.

still extremely low, leading to the work which is presented in this thesis in which, essentially, the Paul trap is replaced by an RFQ ion guide. The benefit of the ion guide derives from fact that it can contain enough gas to bring the ions to rest within the containment device, much more gas than can be contained in a feasible Paul trap. However, the much smaller geometry of the RFQ ion guide compared to the Paul trap places much tighter design requirements on the decelerating system which fits the incoming beam into the structure. The challenge for the work of this thesis was to develop such a deceleration system.

3 Background

The design of a system that decelerates high-velocity ions in a fashion that will allow them to be captured and cooled in an RFQ ion guide with buffer gas requires an understanding of how radio-frequency quadrupole fields capture and confine ions and how buffer gas then cools them. In this chapter, the basic principles of these two phenomena are outlined, as are the consequences in terms of the phase space volume of an ion beam.

3.1 RF confinement

Historical review

Ion confinement was first demonstrated by Penning [7], who used an electrostatic potential well along the axis of a magnetic field. The magnetic field confined the ion motion to be circular about the axis while the electrostatic field confined it to be oscillatory along the axis. Penning used this configuration for the study of ions produced through gas discharge. This kind of trap is now known as the "Penning trap".

However, the lifetime of the ions in this trap was short, of the order of a millisecond. Collisions of the ions with the background gas disturb the centres of the circular orbits away from the axis. Gauss's divergence theorem states that for an axially confining electrostatic field, there must be a radially repulsive field. This repulsive field, acting on the centres of the ions' orbits, drives the ions out of the trap. Therefore, Penning traps with DC electric fields only provide total confinement in the absence of such orbit perturbations.

Paul and his co-workers first achieved total confinement of ions [8]. They simply oscillated the electric field used by Penning. Because the field increases in strength with the distance from an origin where it is zero, the net impulse exerted on an ion over a cycle of the field is not zero. This is because the phase of the forced oscillation of the ion is such that its greatest excursion from the centre occurs when the field is strongest towards the centre and it passes through the centre when the field is strongest away from it. This

results in a net attraction towards the centre. This also holds true for the radial motion. In fact, no magnetic field is required to restrain the radial motion in a trap operated in this fashion. Traps based upon this principle are relatively cheap, reliable, and easy to operate, and have become very common instruments in the modern physical sciences. They are now called "Paul traps".

The properties of the solutions of the equations of motion for a particle exposed to such fields were studied by Mathieu in the middle of the 19th century in the context of the perturbation of planetary orbits. The following section is a summary of the most important features of Mathieu's solutions, as found in mathematical reference books.

Quadrupole electric fields and the Mathieu equation

In vacuum, the motion of charged particles in the transverse plane of a quadrupole ion guide is expressed by the following equation, which is called the Mathieu equation:

$$\begin{bmatrix} \ddot{x} \\ \ddot{y} \end{bmatrix} + \frac{e}{mr_0^2}(U - V\cos\omega_{RF}t)\begin{bmatrix} x \\ -y \end{bmatrix} = 0, \tag{5}$$

where m is the ion mass, r_0 is the distance from the axis to the quadrupole surfaces, U is the DC potential, and V and ω_{RF} are the amplitude and angular frequency of the AC potential, respectively. Since confinement of ions in an electric field requires an oscillation at a radio frequency, the frequency of this oscillation is also referred to as the "RF frequency". By introducing the four dimensionless parameters

$$\begin{aligned} a_x &= \frac{4eU}{m\omega_{RF}^2 r_0^2} \\ q_x &= \frac{4eV}{m\omega_{RF}^2 r_0^2} \\ a_y &= -a_x \\ q_y &= -q_x \end{aligned} \tag{6}$$

and by expressing time in terms of the parameter $\tau = (\omega_{RF}^2 t)/2$, we find the canonical form of the two equations:

$$\frac{d^2 x_i}{d\tau^2} + (a_i - 2q_i \cos 2\tau) x_i = 0. \tag{7}$$

The solutions to these equations are derived and explained in great detail in the literature (e. g. [9]). The stable solutions are of the form

$$x_i(\tau) = A \sum_{n=-\infty}^{\infty} C_{2n} \cos(2n+\beta)\tau + B \sum_{n=-\infty}^{\infty} C_{2n} \sin(2n+\beta)\tau \tag{8}$$

with $0 \le \beta < 1$. This means that they are the superposition of oscillations with the frequencies ω_n, where ω_n is given by

$$\omega_n = (2n+\beta)\frac{\omega_{RF}}{2}; \quad n = 0, 1, 2, \ldots \tag{9}$$

The lowest-frequency component of this oscillation is called the "macro-motion" or also "β-motion"; its frequency is

$$\omega_0 = \beta \frac{\omega_{RF}}{2}. \tag{10}$$

For small values of β ($\beta \le 0.4$), the two lower-frequency components of the oscillation prevail. It is then useful to express the displacement x_i of a particle as the sum of a displacement $\tilde{x}_i$ due to the macro-motion and a displacement δ_i due to the micro-motion:

$$x_i = \tilde{x}_i + \delta_i. \tag{11}$$

If one furthermore assumes that $\delta_i << \tilde{x}_i$, $d\delta_i/dt >> d\tilde{x}_i/dt$, and $a_i << q_i$, Eq. (5) can be solved to give

$$\delta_i = \frac{-q_i \tilde{x}_i}{2} \cos 2\tau. \tag{12}$$

This equation implies that the displacement due to the micro-motion increases linearly with the displacement due to the macro-motion, and that their phases are opposed. When Eq. (12) is plugged back into the Mathieu equation, one obtains equations of motion for $\tilde{x}_i$ that are those of a harmonic oscillator:

$$\frac{d^2 \tilde{x}_i}{dt^2} = -\left(a_i + \frac{q_i^2}{2}\right)\frac{\omega^2}{4}\tilde{x}_i = -\omega_0^2 \tilde{x}_i \tag{13}$$

This provides an elegant way to describe the macro-motion of the particle: Its motion is equivalent to that of a particle in a potential well. In the absence of a real potential well one speaks of a "pseudo-potential well." For the special case of zero DC potential ($U = 0$ and $a_i = 0$), its potential (its depth) is

$$\tilde{D}_i = \frac{q_i V}{8} = \frac{eV^2}{4m\omega^2 r_0^2}. \tag{14}$$

Qualitative description

Figure 6 shows graphs of the numerical integration of Mathieu's equation. The overall restraint exerted on the ions by the oscillating electric field results in a simple harmonic motion, the macro-motion. Its frequency increases with an increase of the RF voltage.

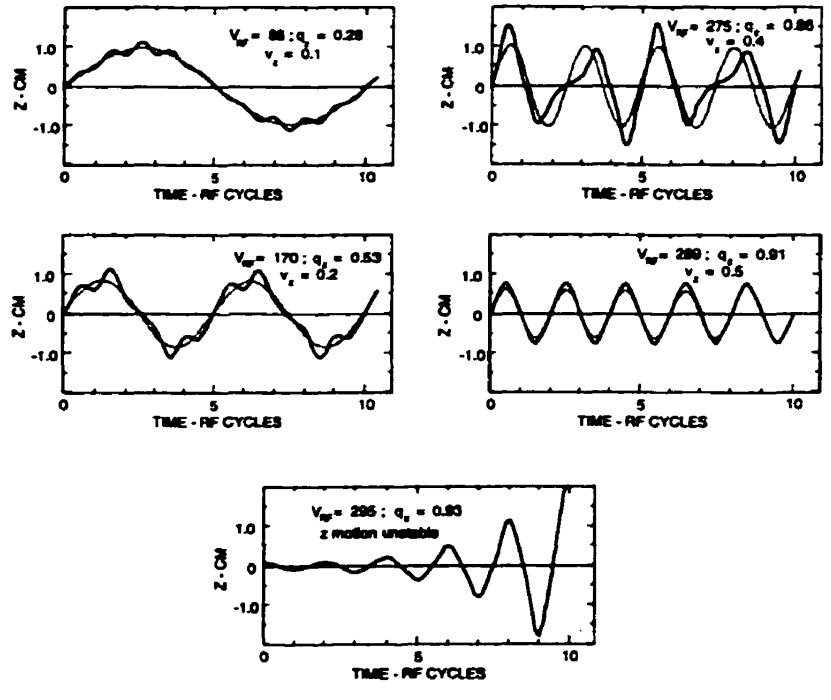

Figure 6: Graphs of the numerical integration of Mathieu's equation for various parameters

The forced oscillatory motion that produces the restraint that results in the confinement is a higher-frequency oscillation that is superimposed on the macro-motion. At low field strengths, its frequency is exactly half that of the oscillating field. This motion is the micro-motion. One can see that the amplitude of this micro-motion is indeed proportional to the radial displacement of the ion due to the macro-motion. Furthermore, the ratio of its amplitude at the peak of the macro-motion to the macro-motion amplitude itself increases with the electric field while, because of the modulation due to the macro-motion, its frequency becomes progressively less than that of the driving electric field.

At a critical value for the electric field strength, the amplitude of the micro-motion of the particle overcomes that of the macro-motion and the motion of the particle becomes unstable. At this point, because of the increase of the frequency of the macro-motion and the concurrent reduction in the frequency of the micro-motion, both frequencies have converged onto exactly half the RF frequency. At the point of instability, the micro-motion and the macro-motion have therefore become indistinguishable.

The dimensionless parameter β which we have encountered in the Mathieu equation was chosen in such a way that it ranges from 0 to 1 for the stable solutions of the equation. It is just twice the ratio of the frequency of the macro-motion to that of the RF field.

3.2 Buffer gas damping and diffusion

While the buffer gas cooling process within the RFQ ion guide did not itself enter into the design of the injection system, the cooling effect is indispensable for the capture of ions in the guide. It will therefore be discussed briefly here.

Historical Review

Buffer gas damping of ion motion in an RFQ trap was first demonstrated by Hugget and Menasian in 1965 for Hg^+ ions in a Paul trap into which a small

amount of helium was introduced [10]. Damping time constants achieved in such devices typically range from about 1 to 100 ms.

The ease with which background gas can be used to cool ion motion in Paul traps led to the study by Douglas and French [11] of the effect of background gas on the transverse motion of ions in a radio-frequency quadrupole rod structure such as used in a quadrupole mass filter. In fact, it was shown that background gas at moderate pressures, up to about 1 Pa, resulted in a significant increase in the transmission of ions through a 1 mm diameter orifice following the quadrupole rods.

This was followed by the work of Taeman Kim, cited above [2], which showed that a transverse radio-frequency quadrupole field could be used to confine ions injected at up to 100 eV and subsequently cooled to close to room temperature by a buffer gas at pressures up to 100 Pa.

Central to the design of devices for such work is information on the drag forces on ions in gases that has been acquired in the long history of the study of ion mobility in gases.

Ion mobility

The concept of ion mobility originated in the late 19th century in the context of the conduction of electricity in liquids and gases, and some of the greatest names in physics have come to be associated with the phenomenon involved. The concept was first introduced by Nernst [12] in the context of the osmotic pressure of liquids. Townsend [13] developed the concept of ion mobility for gases, based on the fundamental paper on kinetic theory by Maxwell [14]. Interest in the subject increased greatly with the discovery by Roentgen that x-rays increased the electrical conductivity of gases, and Thompson received the Nobel prize in physics (1905) for his contributions to the study of such conductivities. By as early as 1905, an accurate quantitative theory of ion mobility was developed by Langevin [15]. Einstein also contributed to the subject by estimating ion mobility from a study of Brownian motion [16], [17].

However, interest in the subject then waned, except as a recurrent theme within the development of technologies such as mass spectrometry and high-voltage electrical breakdown in gases. Interest in the subject itself reappeared, briefly, in the late 1920's in the context of the chemistry of ion-molecule reactions. It reappeared again just after World War II in the context of the ionisation of air by nuclear blasts. Since the mid 1960's, ion mobility has been almost exclusively a subject within chemistry, first in the context of tropospheric and stratospheric chemistry and later in the context of the detection of pollutants in the atmosphere. Since then, many accurate ion mobility measurements have been carried out for specific ions in specific gases and the results have contributed a great deal to the knowledge of the basic nature of ion-molecule interactions [18].

The concept of ion mobility derives from the fact that in low electric fields, the collision rate of an ion with gas molecules does not depend on its own drift velocity while an applied electric field causes it to drift slowly through a gas. This is because the velocities of the thermal motion of the gas molecules are typically much greater than the drift velocity. The average rate of loss of momentum of the ion is the average momentum loss per collision times the average collision rate. If the ion is being dragged in a particular direction by an electric field, then the average field-direction momentum loss per collision is a constant fraction of the momentum in that direction. Because the average collision rate is independent of the electric field, the average rate of loss of momentum in the field direction will be proportional to the ion momentum in that direction. In equilibrium, this average rate of loss of momentum is equal to the average rate of gain from the field. The average rate of gain is simply the electric force on the particle, and so the average ion momentum in the field direction is proportional to the electric field. This relationship is expressed as the drift velocity $\vec{v}_d$ of an ion in a gas being proportional to the electric field $\vec{E}$ in the gas:

$$\vec{v}_d = K\vec{E}, \tag{15}$$

where the proportionality constant K is referred to as the "ion mobility". Its most common units are $cm^2 \cdot V^{-1} \cdot s^{-1}$. Representative values for ions in gases at normal atmospheric pressure and room temperature are from 10 to 20 $cm^2 \cdot V^{-1} \cdot s^{-1}$ for ions in helium and from 1 to 3 $cm^2 \cdot V^{-1} \cdot s^{-1}$ for ions in nitrogen, the higher values being for light ions and the lower values for heavy ions. When expressed in the SI units of $m^2 \cdot V^{-1} \cdot s^{-1}$, these values are, of course, multiplied by 10^{-4}.

The relationship of ion mobility to ion cooling

The fact that the drag force on an ion is proportional to its velocity means that the gas acts on it as a sort of viscous drag. This results in an exponential decay of the velocity, the decay time constant being simply proportional to the mobility. Since the mobility of an ion in a gas is inversely proportional to the gas pressure, the decay time constant is then proportional to the so-called "reduced" mobility (the mobility at standard atmospheric pressure and temperature) and inversely proportional to the gas pressure. For the representative case of a caesium ion in helium at a pressure of 1 Pa, the decay time constant is about 0.3 ms. Since the kinetic energy is proportional to the square of the velocity, the energy decay time constant will be just half this, or about 0.15 ms. This is about 4 orders of magnitude faster than the cooling of high-energy storage beams by electrons.

3.3 Phase space and Liouville's theorem

Phase space

As mentioned in the introduction, the phase space of a collection of particles is the six-dimensional space of the three spatial co-ordinates $x_i(t)$ and the three momentum co-ordinates $p_i(t)$ [19]. In linear systems, the motions in the three orthogonal co-ordinates x_1, x_2, and x_3 are independent of each other. It is then convenient to represent the six-dimensional phase space as its three two-dimensional projections (x_i, p_i). These projections are

called "phase space diagrams." The three orthogonal co-ordinates are chosen in accordance with symmetries of the system.

The phase space area S_i of one phase space diagram is the area which encloses all of the particles in the collection:

$$S_i = \iint dx_i \, dp_i \,. \tag{16}$$

Its unit is the unit of action ($kg \cdot m^2 \cdot s^{-1}$). That is why phase space diagrams are sometimes called "action diagrams". Any other units whose product is the unit of action ("canonically conjugate units") may also be used for the phase space area. In particular, the unit of energy times time (eV·μs) can be useful for expressing the longitudinal phase space area of a collection of particles. The conversion factor between these two units is

$$1\,eV \cdot \mu s = 1.602 \cdot 10^{-25}\ kg \cdot m^2 \cdot s^{-1} \tag{17}$$

Liouville's theorem

The motion of a statistical collection of particles is governed by Liouville's theorem. It states that in the absence of dissipative forces, the phase space of the collection of particles behaves like an incompressible fluid. This means that the six-dimensional phase space volume occupied by the collection of particles will remain constant. Furthermore, in certain systems, the two-dimensional phase space area in all three orthogonal co-ordinates is also conserved. The phase space volume S is then just the product of these three phase space areas:

$$S = \prod_i S_i \,. \tag{18}$$

This is the case when the system is linear and there is no time-varying manipulation of the collection of particles.

The simplest phase space diagrams for a collection of particles are rectangles. These are the phase space diagrams of particles which are uniformly distributed in a sharply-bounded space and have a uniform momentum spread in a sharply-bounded momentum space.

Emittance

The momentum axis of phase space diagrams is often labeled in units of the average (or "central") momentum p_0 and becomes dimensionless. Such a diagram is called an "emittance diagram" and its area is called the "emittance" ξ_i. In terms of the emittance, the phase space area becomes

$$S_i = p_0 \xi_i . \tag{19}$$

The phase space volume is then

$$S = p_0^3 \prod_i \xi_i . \tag{20}$$

3.4 Phase space volume of an ion beam

Emittance diagrams

Emittance diagrams of ion beams are not usually parallelograms. Real beams travelling through cylindrical beam pipes tend to have elliptical emittance diagrams [19]. However, in linear systems, ellipses also remain ellipses. Furthermore, the behaviour of the ellipse can be studied by following through the system the progression of the parallelogram that encloses the ellipse. As an example, the emittance diagrams of a beam passing through a lens are shown in Fig. 7.

For ion beams, the momentum axis of the emittance diagram can be thought of as the angular divergence (in radians) between the ions and the average momentum because

$$\frac{p_i}{p_0} = \tan\varphi_i \approx \varphi_i \tag{21}$$

for small φ_i, where φ_i is the angle enclosed between the momentum of the single ions and the average momentum, projected into the plane perpendicular to x_i. Because of the elliptical shape of the emittance diagrams of beams, the emittance is usually expressed in units of π·mm·mrad, the area of an ellipse being π times the product of its semi-axes.

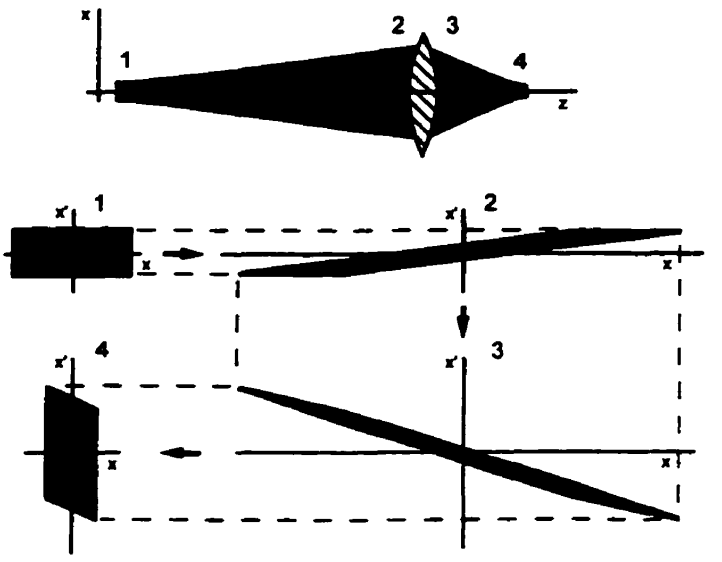

Figure 7: Progression of a beam through a lens (from [19]).

Since the divergences and displacements of particles in a beam usually follow a Gaussian distribution, it is not possible to include all of the particles in the emittance diagrams. Instead, the ellipses are understood to enclose a useful fraction of the particles, out to 2σ of the distribution for example.

Normalised emittance

Because the average momentum p_0 of a beam increases with an acceleration, the emittance of the beam diminishes. In order to preserve the emittance under accelerations, it is often expressed as a "normalised emittance" $(\xi_i)_n$. In a normalised emittance diagram, the momentum axis is scaled by a factor of $\beta\cdot\gamma$, where β is the ratio of the velocity of the particle to the speed of light and γ is the ratio of the relativistic mass of the particle to its rest mass. In terms of the normalised emittance, the phase space area is expressed as

$$\begin{aligned} S_i = p_0 \xi_i &= \frac{p_0}{\beta\gamma} (\xi_i)_n \\ &= m_0 c\, (\xi_i)_n \quad , \end{aligned} \tag{22}$$

where m_0 is the rest mass of one of the particles. The conversion factor between the normalised emittance and the phase space area in a given co-ordinate is

$$S_i = 9.772 \frac{\text{eV} \cdot \mu\text{s}}{\text{u} \cdot \pi \cdot \text{mm} \cdot \text{mrad}} \cdot A (\xi_i)_n \quad , \tag{23}$$

where A is the mass of the individual particles in unified atomic mass units (u) and $(\xi_i)_n$ is the normalised emittance in π·mm·mrad.

Phase space volume of a beam pulse

A continuous beam obviously has a phase space volume of infinite size. One can, however, consider the phase space of a beam pulse. In order to increase the efficiencies of ion traps, continuous beams are usually pulsed ("bunched") before injection into measurement traps.

The longitudinal emittance of a beam pulse can be expressed as

$$\xi_z = \frac{\Delta p \, \Delta z}{p_0}, \tag{24}$$

where Δz is the beam length and $\Delta p \equiv \Delta p_z$ is its momentum spread at a time focus. From Eq. (20), the phase space volume then takes the form

$$S = \xi_x \xi_y \, \Delta p \Delta z \, p_0^2 , \tag{25}$$

or, in terms of the normalised emittances,

$$\begin{aligned} S &= m_0^2 c^2 (\xi_x)_n (\xi_y)_n \, \Delta p \, \Delta z \\ &= m_0^2 c^2 (\xi_x)_n (\xi_y)_n \, \Delta E \, \Delta t . \end{aligned} \tag{26}$$

The conversion factor between the normalised longitudinal emittances and the phase space volume is

$$S = 95.49 \frac{(\text{eV} \cdot \mu\text{s})^2}{\text{u}^2 \cdot (\pi \cdot \text{mm} \cdot \text{mrad})^2} \cdot A^2 \, (\xi_x)_n (\xi_y)_n \, \Delta E \, \Delta t , \tag{27}$$

where A is the mass of the individual particles in unified atomic mass units (u) and ΔE and Δt are the energy spread of the beam pulse at a time focus in eV and the time interval it takes for the beam pulse to pass that focus in μs, respectively.

3.5 Phase space volume of an RFQ trap

Particles in any trap can be considered as a stationary cloud that exhibits some internal motion. While the phase space volume of a stationary cloud can serve as an estimate for the phase space volume of a trap, a full picture of that phase space can only be obtained from the phase space diagrams of the internal motions of the particles in the cloud.

Paul traps

For a cylindrically symmetric Paul trap, the phase space diagrams in the three spatial co-ordinates can be considered separately [19]. The particles follow independent harmonic motions. The phase space diagrams are simply ellipses. If the momentum axes of these diagrams are scaled so that the ellipses become circles, the particles move around in circles with constant angular velocity ω_i in the phase space diagrams.

The micro-motion in a Paul trap is coherent with the driving RF field. It generally doesn't contribute to the phase space volume, but because of it, the slower oscillations of the macro-motion cannot extend out to the physical limits of the trap. The fraction of the physical volume that is available varies with the operating parameters of the trap, but for a typical set of frequencies, the available space in both the radial and the axial co-ordinate direction is about 70 percent of the physical dimensions.

As a consequence of the cylindrical geometry of the trap's containment region, its phase space volume is just the product of the phase space areas in the three spatial co-ordinates:

$$S = \pi^3 m^3 \prod_i \omega_i (x_i)^2_{max}, \tag{28}$$

or, in units of $(\mathrm{eV}\cdot\mu\mathrm{s})^3$:

$$S = 0.0086 \frac{(\mathrm{eV}\cdot\mu\mathrm{s})^3}{\mathrm{u}^3\cdot\mathrm{MHz}^3\cdot\mathrm{mm}^6} \cdot A^3 \prod_i f_i (x_i)^2_{max}, \tag{29}$$

where A is the mass of the individual particles in unified atomic mass units (u) and $f_i = \omega_i / 2\pi$ are the frequencies of their oscillations in MHz.

For the Paul trap, this simplifies to

$$S = 0.0086 \frac{(\mathrm{eV}\cdot\mu\mathrm{s})^3}{\mathrm{u}^3\cdot\mathrm{MHz}^3\cdot\mathrm{mm}^6}\cdot A^3 f_r^2 f_z a_{\max}^6 , \qquad (30)$$

where $a_{\max}$ is the maximal allowable amplitude of the macro-oscillation in the Paul trap.

RFQ ion guide

An ion guide is of indefinite length, in the sense that while particles still enter its front end, other particles may already be leaving the rear end. The phase space volume of an RFQ ion guide is therefore not defined. The important quantities are the phase space areas in the transverse co-ordinate directions.

The acceptance diagram of an RFQ ion guide at any given time is an ellipse. But because of the phase of the RF potential, the ellipse constantly rotates. There is no means of matching such a rapidly varying phase space ellipse with an electrostatic decelerating electrode. One must therefore make sure that the phase space ellipse of the ion beam is smaller than the acceptance diagram of the RFQ ion guide for any given phase. This means that the simulation of the injection into the ion guide must be carried out for a number of different phases. If the phase space of the beam turns out to be larger than the acceptance diagram of the RFQ ion guide for a given phase, then particles are lost. If this is the case only for a small fraction of the RF phases, then a slight loss of particles may be accepted.

3.6 Twiss parameters

The general equation for an ellipse that is centred on the origin is

$$By^2 + 2Axy + Cx^2 = \varepsilon , \qquad (31)$$

where ε is the product of the semi-axes of the ellipse. The four parameters A, B, C, and ε are called the "Twiss parameters" of the ellipse.

Figure 8 shows the relationship between the Twiss parameters and the four critical points of an ellipse. These relationships can also be solved for the

Twiss parameters. This is how the parameters of the phase space ellipse of a collection of particles can be extracted from their emittance diagram.

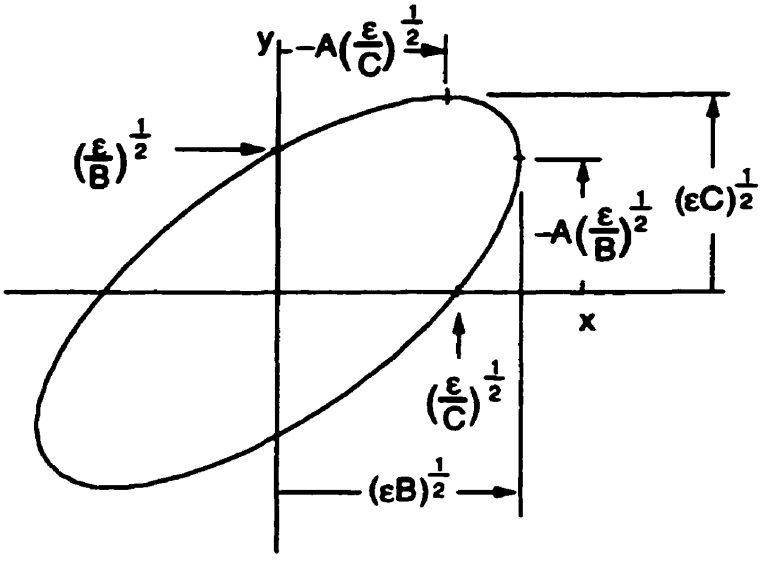

Figure 8: Relationship between the four critical points of an ellipse and its Twiss parameters.

3.7 Design goals / requirements

As pointed out above, the design goal for the decelerator developed in this work was, basically, to be able to render a typical ISOLDE beam into a form that could be captured in a feasible RFQ ion guide. In phase space terms, this means that the phase space diagrams of the decelerated beam must fit within the acceptance diagram of the RFQ guide. For this, a representative ISOLDE beam was taken to be caesium (of atomic mass 133 u) at 60 keV and to have an emittance of 30 π·mm·mrad and an energy spread of 5 eV. The aim of the deceleration was to produce a beam with a phase space diagram that could be accepted by the ion guide. The development of a feasible design for this was an iterative process in which the effect of a variety of electrode configurations on the incoming ion trajectories was numerically simulated by a variety of procedures.

4 Computer simulation

4.1 Simulations performed at McGill University

Principle

The simulations which are described in this section were the starting point of this project. Their goal was to establish a geometry for a deceleration system and an RFQ ion guide that meet the requirements put forth in the previous chapter.

The computer code that was used consists of four distinct parts, all of which were developed by our group. The first three of these parts were developed at McGill University for other purposes, while the fourth, the matrix method simulation of the low energy beam entering the RFQ ion guide, was written specifically for this project by Peter Varfalvy.

As had been shown by the work of Kim [2], an RFQ ion guide with buffer gas is able to cool ion beams at energies of up to about 100 eV. It was therefore possible to separate the simulation into two distinct steps:

1. The deceleration and focusing of the 60-keV ion beam to energies approaching 100 eV while at the same time carefully matching its phase space properties to the following RFQ ion guide.
2. The injection of the decelerated beam into the RFQ ion guide.

Deceleration and focusing

The simulation code for the design of the deceleration and focusing electrodes consists of two parts: a two-dimensional relaxation code for determining the electric field in the volume of interest, and a Runge-Kutta integration for the calculation of trajectories of single ions in this field. Both codes are extensions of principles introduced and explained in [20]. The Runge-Kutta code was written by Peter Varfalvy and is explained in detail in his thesis [21]. A feasible design for a decelerator for the purpose of the present work requires a great variation in the electric field strength over short

distances. In order to achieve sufficient accuracy in the simulations of such structures, the technique of "adaptive step size control" had to be implemented. This allows the step lengths to automatically be adapted to the changing electric field and expands the accuracy of the Runge-Kutta integration from fourth-order to fifth-order.

The Runge-Kutta numerical integration calculates the trajectories of a grid of particles in the two-dimensional transverse phase space. Because of the axial symmetry in that region, the second transverse phase space co-ordinate need not be considered. Typically, the number of particles studied varies between 9 and 25. The output of the program is the evolution of the phase space co-ordinates of all of these particles as a function of time t and the axial co-ordinate z. It can be graphically displayed as time-varying scatter plots of any two co-ordinates, or simply as an evolution of the trajectories of all particles. A change in geometry always requires a new calculation of the electric fields, whereas a change in the electrostatic potential amplitudes is achieved by simply scaling the result of the relaxation, which is always normalised to unity at the outset.

At the beginning of the design phase, the electrostatic deceleration and injection part of the apparatus was expected to require the least amount of work and time. A single conical decelerating electrode was to be used for the complete deceleration of the 60-keV beam to an energy of about 100 eV, while at the same time providing a small aperture of no more than 6 mm diameter which allows the large pressure gradient which is necessary for efficiently evacuating the deceleration region. But as had become obvious from the performance of such a system in the very large Paul trap at the ISOLTRAP experiment, such a simple approach would not yield the efficiencies required. After tens of simulation runs with different geometries and careful evaluation of the results of those simulations (in terms of the six-dimensional phase space of the resulting beam), a novel design for such an electrostatic deceleration electrode slowly crystallised.

Decelerating an ion beam as strongly as needed to be done here always leads to a sharp focus. Of course, the focus must be very close to the exit aperture of the electrode, otherwise most of the ions hit the electrode, either before or after the focus. When a beam is decelerated in a linear system, its overall transverse phase space volume remains constant. Because the central energy is greatly reduced, however, the transverse emittance increases. This is an effect which cannot be overcome without dissipative cooling. There is, however, another effect which contributes to an increase of the transverse phase space: In a non-linear system, the phase space area in the axial co-ordinate direction is not separately conserved. Part of the longitudinal momentum is transferred to transverse momentum. This effect must be minimised in the design of a system of decelerating electrodes. This can only be achieved – if one restricts the solution to a single electrode – with an electrode with the largest possible initial diameter.

Eventually, however, the electrode must close in onto the axis in order to form the aperture. This must not happen too abruptly. We have found that the surface formed by a quarter ellipse, offset from the axis by the radius of the aperture, and rotated around the z axis, assures a minimal transfer of the longitudinal momentum to the transverse momentum. The optimal length of this ellipse for any given height is found by varying the length until the focus of the decelerated beam comes to lie very close to the aperture. The exact location of the focus is subject to additional considerations such as further decelerating stages. In addition to the ellipse, we have done simulations with a great number of other shapes for the decelerating electrodes, always keeping the initial diameter constant. None of the shapes studied (combinations of cones, parabolae, hyperbolae) delivered a beam with as little divergence as the elliptical electrode.

Thus it can be seen that the initial diameter of the decelerating electrode must be as large as possible. In reality, that diameter is obviously limited by the beam pipe and the necessary distance from the electrode to the beam pipe in order to prevent electrical spark-overs from the decelerating electrode

to ground. It became clear that with a beam pipe such as the ones which are used throughout the experimental set-up at McGill University as well as at CERN (100 mm diameter), one deceleration stage was not sufficient for delivering a beam of low enough divergence to be injected directly into the rod structure. Therefore, a second deceleration stage was added in the form of a thin plate with an aperture of the same size as that of the decelerating electrode. Because of the relatively small deceleration but strong focusing caused by this electrode, we generally denote it as the focusing electrode.

Figures 9–11 show the results of the Runge-Kutta calculations for the same geometry, but for different potentials on the electrostatic electrodes. Figure 9 shows the result for a potential which is too high (the negative offset is too small). The focus lies before the aperture, and most ions are reflected back or hit the decelerating electrodes. In Fig. 10, the potential is not high enough (the negative offset is too large). The focus lies far behind the decelerating electrode, and there is no second focus at the focusing electrode. Figure 11 shows the results of the simulation for the optimal parameters. At the axial point where the focusing electrode is located, the ions are bent back towards the axis sufficiently to prevent them from hitting the rod structure. The second focus is stronger than the first one, but it occurs only when the ions have already reached the RFQ ion guide. The potentials that were extracted from this simulation are 57,850 V, 59,900 V, 59,900 V, and 59,950 V for the decelerating electrode, the focusing electrode, and the first and second ion guide segments, respectively

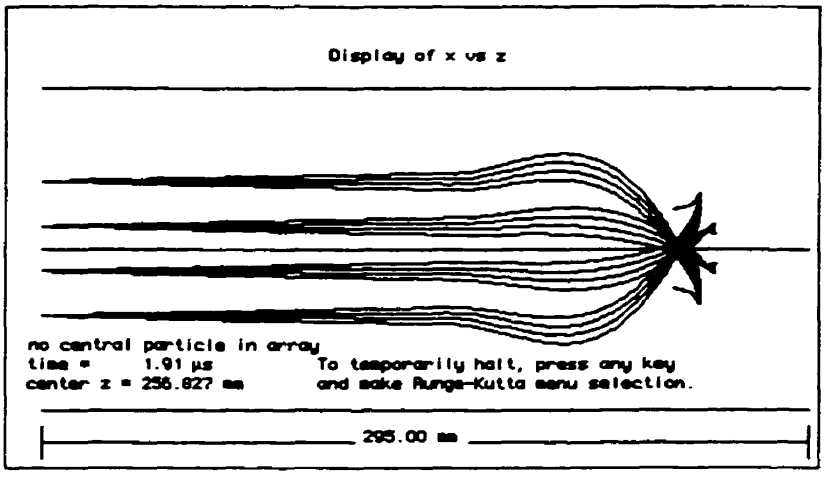

Figure 9: Runge-Kutta simulation of the ion trajectories for too high a positive potential on the decelerating electrode.

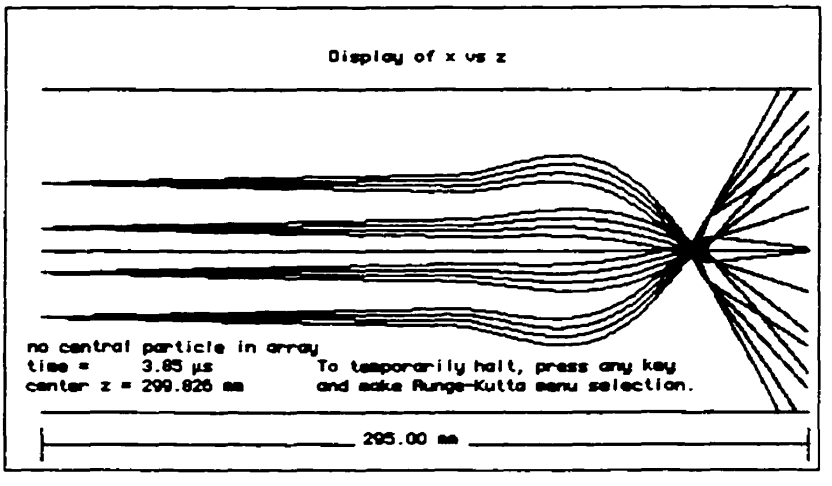

Figure 10: Runge-Kutta simulation of the ion trajectories for too low a positive potential on the decelerating electrode.

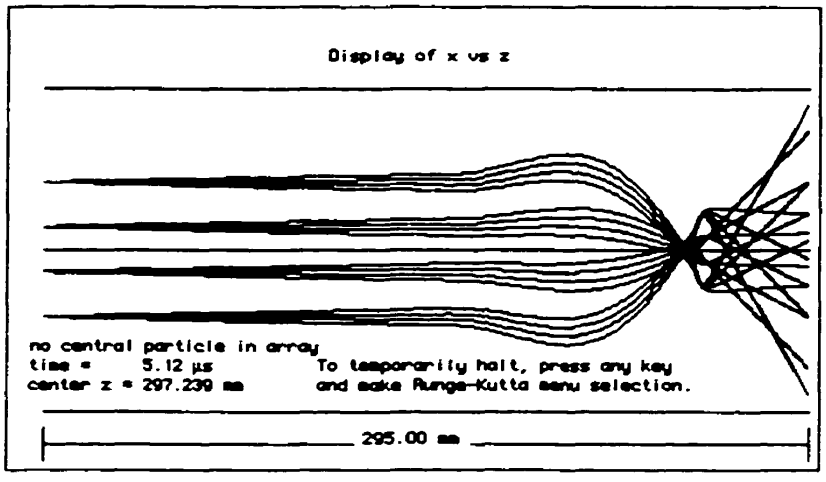

Figure 11: Runge-Kutta simulation of the ion trajectories for a positive potential of 57,850 V on the deceleration electrode.

Once these potentials were established, the Twiss parameters of the transverse phase space ellipse were extracted a few millimetres before the aperture of the decelerating electrode, in order to account for the effect of the RF potential as soon as it starts to play an important role, in the following matrix method simulation. The extraction of the parameters was done manually by fitting an ellipse into the grid of particle co-ordinates in a plot of the transverse phase space. If similar simulations are to be conducted again, it is planned to write code for the automatic extraction of the Twiss parameters from the result files of the Runge-Kutta simulation.

Injection into the RFQ ion guide

This part of the simulation consists of a three-dimensional relaxation of the geometry of the last 20 millimetres of the electrostatic deceleration system and the first three segments (or 60 mm) of the RFQ ion guide. The relaxation code was written by Van Fong for the project described in [2]. It is based on an algorithm presented in [20], extended to three dimensions.

The code which was used to calculate and display the trajectories of the ions in this region was written by Peter Varfalvy specifically for this project. That code was based on an existing spreadsheet calculation technique developed by Prof. Robert B. Moore. With the four Twiss parameters

extracted from the Runge-Kutta simulation at a given point (usually after the first but before the second focus), and as a fourth parameter the central energy of the beam at the same point, this simulation calculates the motion of beam envelopes at different phases (typically 20 phases) into the RFQ ion guide. The output is a graphical view of the overlapping beam envelopes in the *x*-*z* plane. At $z = 250$ mm, the following Twiss parameters were extracted from the Runge-Kutta simulation: $A = -0.6303$, $B = 0.03934$, $C = 35.519$, and $\varepsilon = 9.322$. The central beam energy at the same position was $E_{centr} = 1921$ eV.

Figure 12 shows the results of this simulation for the set of parameters which was found to be optimal. The voltages on the decelerating electrode, the focusing electrode and the first two segments of the ion guide were 57,850 V, 59,900 V, 59,900 V, and 59,950 V, respectively (as for the Runge-Kutta simulation naturally). The RF potential was 300 V peak-to-peak and the RF amplitude was 1.2 MHz. The electrode geometry is shown in the display of the simulation program, but as an indication only. Please note that the decelerating electrode is not accurately represented here. This has no influence on the results of the simulation.

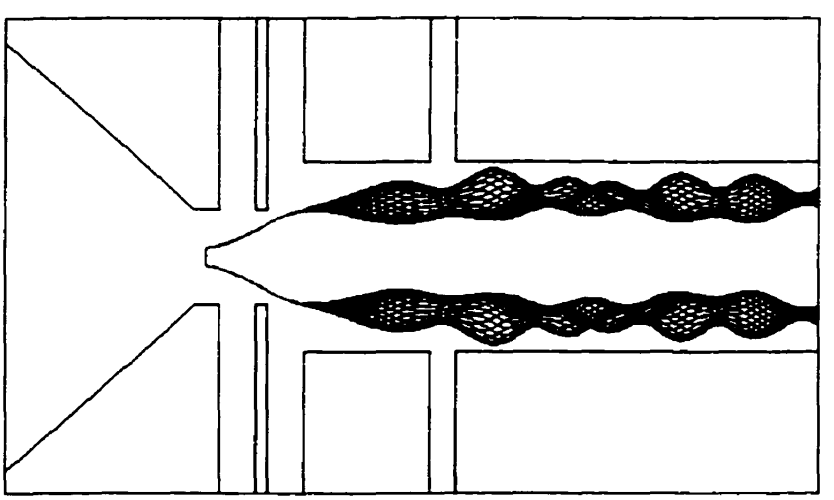

Figure 12: Result of the matrix method simulations for the optimised parameters.

It is obvious from the graphical result that *to first order*, all of the particles which were included in the ellipse extracted from the Runge-Kutta simulation

are successfully injected into the RFQ ion guide for these parameters. As was mentioned before, this is equivalent to about two thirds of a realistic ISOLDE beam with an emittance of 30 π·mm·mrad. It is important to note, however, that the matrix method calculation of the ion trajectories is not conclusive in showing that the RF confinement of the beam in the ion guide will work. It is only a first-order calculation. All higher-order effects (and there can be expected to be important higher-order effects in the focusing region) are not considered. This simulation is therefore an indication that the proposed geometry *may* work. On the other hand, a negative result of this simulation would show that a given geometry *cannot* work.

The important advantage of this method as compared to code that takes into account higher orders of the electric field is its speed. It is possible to simulate the progression of the beam envelope through the whole low-energy injection region in a calculation time of only a few seconds on a Motorola 68040 25-MHz processor. More thorough methods can and should supplement it, but with calculation times of twelve and more hours on much faster processors, they cannot be used for design work where parameters have to be frequently changed in the optimisation process.

Results

Figure 13 shows the geometry such as it was retained for the experimental set-up. The apparatus at McGill University and that at ISOLTRAP have the exact same geometry. In fact, the decelerating electrode now in use at CERN was also built in the physics department's machine shop at McGill University.

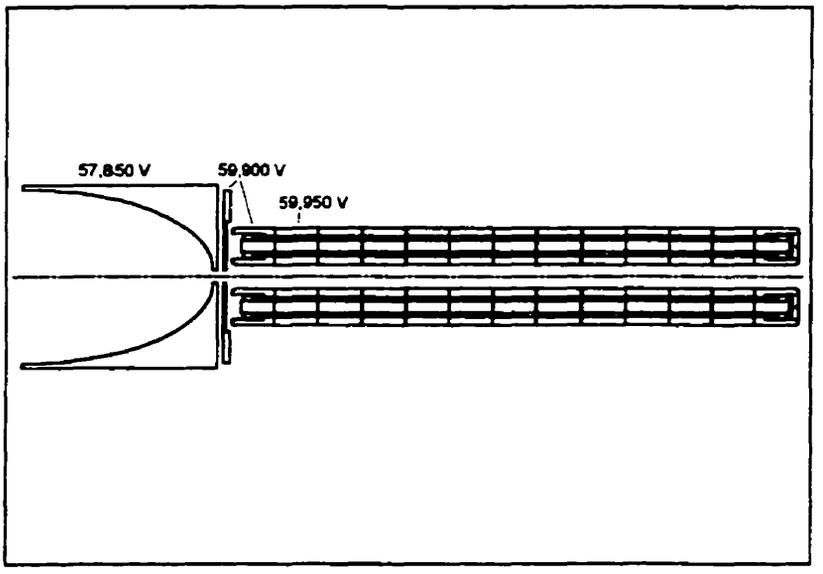

Figure 13: Geometry and voltages as obtained from the simulations. The total length of the components shown here is 355 mm.

4.2 Simulations performed at CERN

In September and October of 1998, with the experimental set-ups both at McGill University and at CERN almost completed, additional simulations were performed at CERN [22] in order to test the design.

Principle

The code used for these simulations is a combination of the commercial software "SimIon" from Lockheed Idaho Technologies and code developed by the ISOLTRAP group at CERN. The following differences distinguish the code from our matrix method simulations:

- The effect of the buffer gas on the ions was taken into account.
- The simulations are higher-order numerical integrations, as opposed to the second-order matrix method we used.
- A realistic phase space distribution for the beam is used, as opposed to considering the beam envelope only.

On the other hand, one run of the code with one set of parameters takes about 12 hours on a Pentium-II 350-MHz processor. This is the reason why such a code cannot be used in an initial design phase, but only once

approximate design parameters have been established by some other means. The geometry that was used corresponds exactly to the system at McGill University, with the exception that the axial distance between the focusing electrode and the first segment of the ion guide was taken to be 5 mm instead of 3 mm. The ion motion was pursued up to and including the sixth set of segments of the RFQ ion guide.

The potentials on the decelerating and on the focussing electrode, the DC potentials on the six sets of segments, as well as the RF potential amplitude and frequency were varied in order to study their effect on the efficiency of the system. The energy of the incoming beam (60 keV), the buffer gas pressure (200 mPa), and the type of ions (^{133}Cs) were left unchanged for this simulation. Initially, the longitudinal distance between the ground cylinder and the decelerating electrode was also varied in the simulations. After high voltage tests showed that the configuration such as designed at McGill University posed no problems of spark-over, only the configuration with zero axial distance was used.

In all of the runs, the following phase space of the incoming beam was examined:

$$-3\ \text{mm} \le x_i \le 3\ \text{mm} \quad \text{and}$$

$$-10\ \text{mrad} \le \varphi_i \le 10\ \text{mrad}.$$

For reasons of symmetry, only one eighth of that phase space needs to be calculated.

Results

The results of these simulations are output in the form of efficiencies for transverse phase space elements in the four-dimensional volume $(x, \varphi_x, y, \varphi_y)$.

Since the initial distribution of particles in that volume is that of the ISOLDE beam, the total efficiency of the apparatus is just the average of the efficiencies for all volume elements. Table 1 shows the global efficiencies for different potentials on the deceleration electrode. The potentials are listed as

relative potentials with respect to the cage high voltage of 60 kV. All other parameters were kept constant.

Relative potential (V)	Global efficiency (%)
–1500	12.88
–1700	29.21
–2150	24.19

Table 1: Global efficiencies through the deceleration stage for different deceleration electrode potentials

Another way of presenting these results is shown in Fig. 14. The graph shows the efficiencies as shades of grey as a function of the transverse spatial co-ordinates. For every data point in space, the efficiencies are summed up over all divergence values. Such diagrams are called "acceptance diagrams." Figure 14 was obtained with the following parameters: Relative deceleration electrode potential –1700 V, relative focusing electrode potential –100 V, and relative DC potentials on the first six sets of segments –70 V, -20 V, –10 V, –2 V, –4 V, and –6 V, respectively.

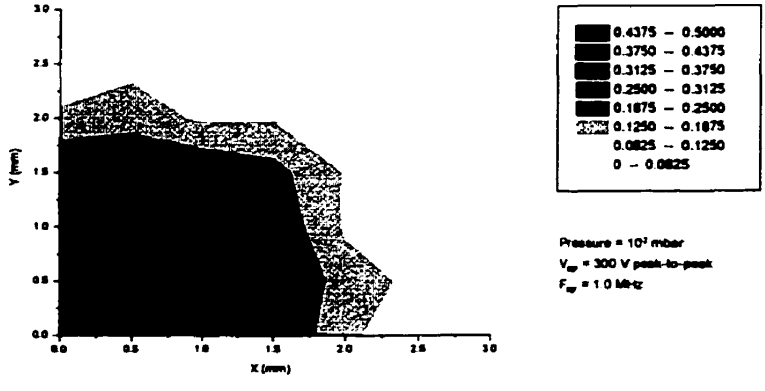

Figure 14: Acceptance diagram for the entire deceleration system and RFQ ion guide up to the sixth segment [23]

The result to retain from these simulations is that the efficiency was found to be highest for the geometry as well as the parameters that are practically

identical to the ones determined from our simulations at McGill University. That maximal efficiency is close to 30 percent.

5 Data and results

5.1 Apparatus

Overview

All parts for the apparatus used at McGill University as well as the electrostatic deceleration system now installed at CERN were entirely designed and machined at McGill University. All of the components of the trap system are made out of stainless steel. Detailed technical drawings of most of the parts are included in Appendix A.

Figure 15 shows an overview of the deceleration apparatus used. The leftmost vacuum element is a so-called "vacuum break", which is a ceramic cylinder with two stainless-steel vacuum flanges across which a potential difference of up to 60 kV can be maintained. All the components to the right of the vacuum break are floated at high voltage in a cage. This is how the deceleration potential is applied to the various electrodes. The electrodes are connected to small HV power supplies that offset them to desired negative potential relative to the cage potential. Communication to digital-analogue converters (DAC's) for control and analogue-digital converters (ADC's) for read-out was fed through several full-duplex fibre-optical links.

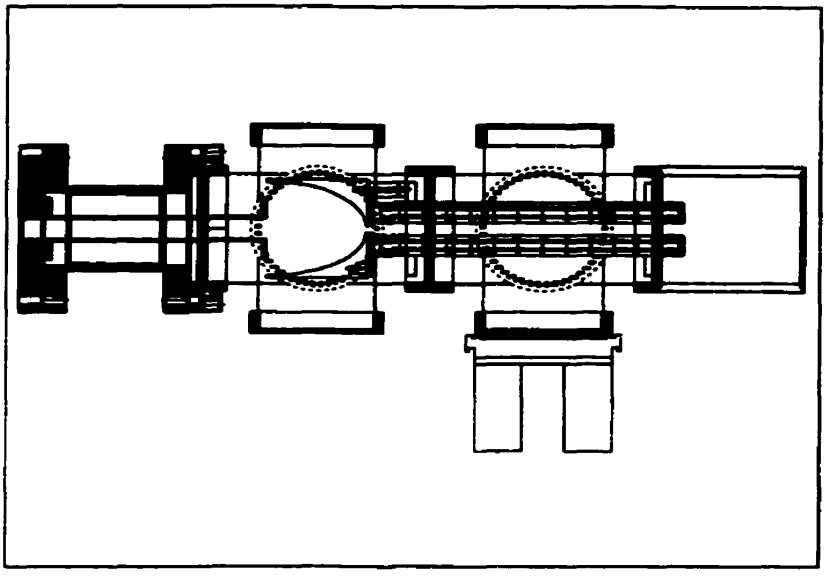

Figure 15: Overview of the deceleration apparatus. The overall length of the components shown here is about 700 mm.

Ion source

The ion source that was used for the measurements made at McGill University was essentially built by a summer student during the summer session of 1997. Its main components are identical to those of an ion source that was built by our group in 1995 and that is now in operation at the ISOLTRAP experiment. Its principle and engineering details are explained in [24] and will not be repeated here.

Ground cylinder

As the ions enter the vacuum break, they must be protected from the electric field due to the high voltage until they reach the designated deceleration region. This is done with a grounded cylinder that extends through the vacuum break into the high voltage region. At the exit of the ground cylinder, the part extends out in the form of a disk up to a distance of 5 mm to the decelerating electrode.

Decelerating electrode

The primary decelerating electrode was machined out of a solid cylinder of diameter 87 mm and of height 90 mm. The machining of the inner volume was performed on the physics department's own CNC (numerical) milling machine using a ball-point milling tool. This operation alone took about 28 hours of uninterrupted machining on the CNC machine. A total of three identical primary electrodes were manufactured, one of which is now in operation at the ISOLTRAP experiment at CERN. For the experimental set-up at McGill University, the decelerating electrode had to be further machined. Due to space constraints, the main pump was mounted directly underneath the decelerating electrode. Therefore, in order to assure the necessary differential pumping, the electrode had to be perforated. A total of 36 radial holes were machined into the decelerating electrode. On the inner electrode surface, the holes were not allowed to overlap, because otherwise the shape of the electric field due to the electrode would have been severely distorted.

Focusing electrode

The focusing electrode was machined out of a disk of diameter 87 mm and thickness 3 mm. Near the aperture, its thickness was further reduced to achieve the shape that had been determined in the simulation.

RFQ ion guide

The ion guide consists of 26 sets of four hollow segments that form four rods. These rods are mounted in mounting plates that also hold four solid ground rods and eight insulating ceramic rods. The grounded rods and the insulating rods are arranged in such a way that the beam never "sees" the insulating rods, where space charges may build up.

The purpose of the axial ceramic rods was to close up the structure into the equivalent of a hollow cylinder. This improves the ratio of the pressure in the ion guide to that in the decelerating region, because the gas can only flow along the central region of the ion guide.

RF coupling circuit

A circuit was designed that permitted the coupling of the DC and RF potentials on the rod segments, and that also featured resistor networks that divided the DC potentials evenly between those points where a DC potential was defined by a HV power supply. I will not go into the details of that circuit here, but it is important to mention that such circuits have resonances. Because of the large number of passive components in those circuits, it is not easily possible to predict the resonant behaviour of the circuit. Because of the limited power that can be delivered by standard RF amplifiers, the circuit must be operated at or near a resonance, otherwise the necessary RF amplitude cannot be reached.

The one component that has the largest influence on the resonance frequency of the circuit is the transformer. However, it is very time-consuming to frequently wind transformers with hundreds of turns. The circuit used for the experiment at McGill University had a resonance frequency of 610 kHz. Therefore, even though that is only about half of the RF frequency that was found to be optimal in the simulation, we had to use the circuit at that frequency. There was no time to optimise that component of the experiment. In order to conserve the β value of the ion guide, we also lowered the amplitude of the RF potential correspondingly to about 115 V peak-to-peak.

Faraday cup detector

The detector that was used to measure the ion current at the exit of the ion guide is a simple Faraday cup detector of about 15 mm diameter. It was mounted on a flange that closed up the vacuum system behind the ion guide. The Faraday cup and the flange are not shown in Fig. 15. Axially, the Faraday cup was located at about 20 mm after the exit of the ion guide.

5.2 Measurements performed at CERN

On 17 December 1998, the day before the annual winter shutdown of ISOLDE, we were able to perform the following measurements at the ISOLTRAP facility at CERN.

Principle

Using the hot plasma ion source, a stable (*i.e.* non-radioactive) ^{40}Ar beam was selected and directed to the ISOLTRAP experimental area. Its current was measured to be 80 nA with a Faraday cup near the experimental set-up. Due to a lack of time, very little effort was spent on optimising the beam. Its emittance was estimated to be at least 35 π·mm·mrad, and especially its angular adjustment was bad.

The decelerating electrode and the focusing electrode were separately connected to high-voltage DC power supplies, whereas the leads to the first 17 sets of segments (*i.e.* the first 33 cm) of the ion guide were shorted together and grounded (to the cage ground) through a pico-ammeter. In this way, we were able to measure the current of ions deposited on the rods of the ion guide and thus determine the ratio of the beam which was successfully injected into it. Let me note here that the current measured on the rods is in any case smaller than the total current injected into the ion guide. That is because a certain number of ions, namely those that have the smallest transverse momentum at the entrance to the ion guide, manage to pass through it without hitting any of the first segments. Furthermore, a small fraction of the ions is also deposited on the grounded rods directly without passing through the ammeter and is therefore not measured.

The principle of the measurement was to vary the electrostatic potentials on the decelerating electrode and on the focusing electrode (independently) in such a way that the current on the rods would be maximised. Since the ion guide segments were grounded as opposed to being at a small negative potential (≤ 100 V), the cage high voltage potential was not raised to 60.0 kV, but only to 59.9 kV. This also means that the electrode potentials which were found to maximise the current on the rods would have to be about 100 V more negative in real operation.

Results

Tables 2 and 3 show the results without and with buffer gas in the ion guide. For the measurement with buffer gas, the buffer gas pressure inside the ion guide was 110 mPa ($1.1 \cdot 10^{-3}$ mbar), the pressure in the region before the decelerating electrode 2.5 mPa ($2.5 \cdot 10^{-5}$ mbar). This compares to a pressure of 0.51 mPa ($5.1 \cdot 10^{-6}$ mbar) in the ISOLDE beam line. In both cases, when the potentials on the electrodes were exchanged, the current disappeared.

Decelerating electrode potential (V; absolute)	Focusing electrode potential (V; absolute)	Ion guide potential (V; absolute)	Current on ion guide rods (nA)	Percentage of incoming beam injected
0	0	0	11	13.8 %
57,900	59,450	59,900	8.6	10.8 %
58,300	59,500	60,000	8.1	10.1 %

Table 2: Maximised current measured on the ion guide rods for various potentials on the electrostatic electrodes. Measurement without buffer gas.

Decelerating electrode potential (V; absolute)	Focusing electrode potential (V; absolute)	Ion guide potential (V; absolute)	Current on ion guide rods (nA)	Percentage of incoming beam injected
56,900 ...57,900	59,275	59,900	7.7	9.6 %
57,000 ...58,000	59,300	60,000	7.6	9.5 %

Table 3: Maximised current measured on the ion guide rods for various potentials on the electrostatic electrodes. Measurement with buffer gas.

These measurements unfortunately contain no information on the efficiency of the RF containment of the ions. They provide no conclusive proof that ions can be trapped in the RFQ ion guide. However, the fact that a large portion of the beam is injected into the physical volume of the ion guide suggests that the electrostatic electrodes efficiently focus and decelerate the beam.

5.3 Measurements performed at McGill University

Principle

In January of 1999, the apparatus which was built at McGill University was ready for operation. All components were operational, but a few problems remained.

One was the fact that it was impossible to operate the ion source beyond about 45 kV because of spark-overs. Since a very similar source has been in operation at ISOLTRAP for many years, we are confident that this is a problem which can be fixed eventually, but it was decided that the measurements should simply be made at a lower potential. The DC potentials on the electrostatic electrodes and the ion guide segments then simply scale. For the measurements described below, the potentials were set to $(V_{cage} - 1133\,V)$ for the decelerating electrode, $(V_{cage} - 133\,V)$ for the focusing electrode, and $(V_{cage} - 67\,V)$ for the first segment of the ion guide. The fifth segment of the ion guide was raised to a DC potential of $(V_{cage} + 23\,V)$, the last segment was raised to $(V_{cage} + 18.5\,V)$. The other electrostatic potentials on the ion guide were automatically divided between these fixed points by the resistor network in the RF coupling circuit. Figure 16 shows the electrostatic electrodes and the ion guide along with the DC potentials that were applied on them.

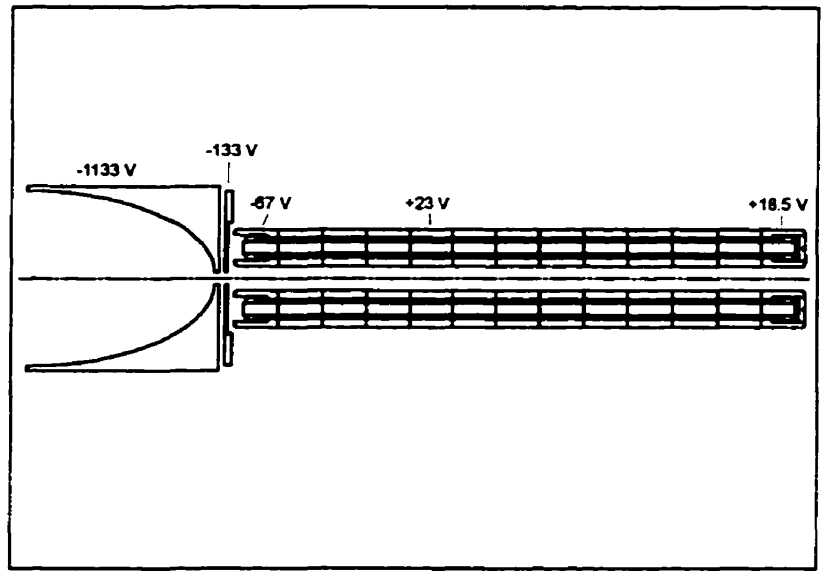

Figure 16: Relative DC potentials (with respect to cage HV) applied to the various electrodes for the experiment.

With this arrangement, once the ions made it past the fifth segment, they were then dragged along the axis up to the Faraday cup beyond the ion guide. The Faraday cup was biased by +9 V with respect to the beam pipe in order to avoid multiple counting of ions from the effect of electrons that are knocked out of the surface of the Faraday cup by incident ions.

Another problem was a short-circuit that was discovered between the first and the second segment of the ion guide, on one phase only. Again, it was decided to leave the very time-consuming correction of that problem for later work. We did not check the effect of this "longer first segment" in a simulation. One can assume, though, that the capture efficiency is slightly decreased.

As was mentioned before, the RF was operated at a frequency of 610 kHz and a potential of 115 V peak-to-peak, which corresponded to an input potential to the RF amplifier of 54 mV peak-to-peak.

In order to see the effect of the buffer gas on the transmission rate, some of the measurements were done with buffer gas and some without. In the absence of buffer gas, the base pressure near the ion guide was below 2.5 mPa ($2.5 \cdot 10^{-5}$ mbar), and below 70 µPa ($7.0 \cdot 10^{-7}$ mbar) in the deceleration region. For the measurements with buffer gas, we set the pressure near the

ion guide to about 80 mPa ($8.0 \cdot 10^{-4}$ mbar). The pressure in the deceleration region then increased to about 13 mPa ($1.3 \cdot 10^{-4}$ mbar).

The principle of the measurement was to slowly raise the potential of the cage (cage HV) from ground up to and slightly beyond the potential of the ion source. This sweep was done several times with the RF on and with buffer gas in the ion guide, twice with RF but without buffer gas, and once *vice versa*.

Results

When the ion source is operated at 40 kV and the cage HV is at ground potential, a fairly constant current is detected on the Faraday cup. This current can be made to vary between about 60 and about 400 pA when the heater current is adjusted in its operating range of about 55 to 60 A.

As we raised the cage HV for the first time, we found a very large negative current, more than 2000 pA, on the Faraday cup. This current was clearly a function of the beam intensity, but practically independent of the buffer gas pressure. We assumed that it was caused by electrons that were knocked out of the ground cylinder, either by stray ions as they entered the deceleration region, or by ions that were reflected back off the decelerating electrode and then hit the ground cylinder. Such electrons would see the large positive potential on the decelerating electrode and be accelerated through the aperture and the ion guide onto the Faraday cup. This hypothesis was quickly proven correct when we placed a magnet outside the beam pipe near the entrance of the ion guide. The negative current disappeared. The electrons were apparently deviated sufficiently from their path to not hit the Faraday cup at the far end of the ion guide any more. The ions, on the other hand, with a mass more than five orders of magnitude greater than that of the electrons, are practically unaffected by the magnetic field.

Although the ion source is fairly stable, the current sometimes varied by a few percent during the time it took to raise the cage HV up to 42 kV and to lower it back down to ground afterwards. For the results recorded here,

however, the ion source current did not vary by more than a few percent between the start and the end of a cycle.

Figure 17 shows the results of the sweeps of the cage HV with the RF turned on but with the buffer gas turned off. As could be expected, the current of the ions that make it all the way through the electrostatic electrodes and the RFQ ion guide diminishes with an increase of the cage HV. There is a slight bump in the curve when the cage HV is near the ion source HV, but the increase in transmission is insignificant. When the cage HV is higher than the acceleration potential of the ion source, all ions are reflected back and none are transmitted.

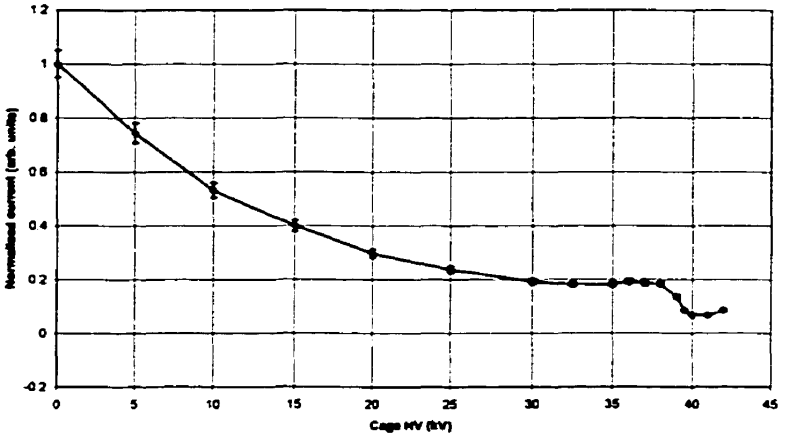

Figure 17: Current measured on the Faraday cup as a function of the cage potential. The RF was turned off and buffer gas was present in the ion guide. The buffer gas pressure was 80 mPa.

Figure 18 shows the same measurements, but with the RF on the RFQ ion guide turned on. When compared with Fig. 17, Fig. 18 strikingly shows the effect of the RF field on the ability of the ion guide to capture and cool the ions. One can clearly identify a strong peak in the transmission for a cage potential that is very close to the ion source potential. This is due to the fact that the potentials on the electrostatic electrodes (relative to the cage ground) were chosen in such a way that they provided a maximal transmission rate when the cage HV was at or very near the ion source HV. The figure also

shows that the maximal transmitted current (at the peak) is of the order of the current that is transmitted when the cage HV is zero. Both in Fig. 17 and in Fig. 18, the error bars represent an estimated 5 percent error which corresponds to the accuracy achievable with the pico-ammeter. Additional systematic errors, such as a negative offset due to a residual electron current, are not shown in the graph. None of these should, however, affect the ratio of the peak current to the initial current.

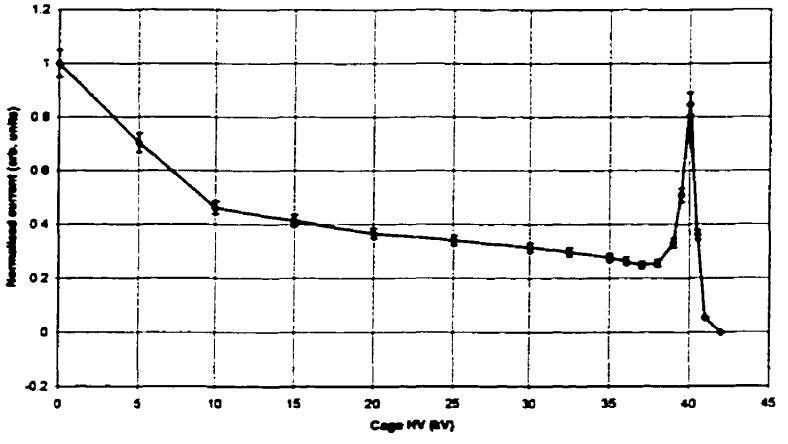

Figure 18: Current measured on the Faraday cup as a function of the cage potential. The RF was turned on and buffer gas was present in the ion guide. The buffer gas pressure was 80 mPa.

When the RF is turned on but no buffer gas is present in the RFQ ion guide, the measured current curve very much resembles the one in Fig. 18. But as would be expected, the ratio of the peak current to the initial current is much higher than with buffer gas. That is because a certain fraction of the particles is removed from the ion trap region in collisions with the buffer gas molecules. Of course, without any buffer gas, the ions cannot be cooled in the radial direction.

These results show that a considerable ratio of the ions produced by the ion source are successfully injected into the ion guide where they are decelerated and cooled. Unfortunately, our set-up didn't allow for a Faraday cup to be moved into the beam before the decelerating electrode in order to measure

the actual ion current from the ion source. However, with a reasonable assumption of what ratio of the ion current is transmitted through the entire structure, the total efficiency of the deceleration system and the RFQ ion guide can be estimated. From a knowledge of the quality of the produced beam, I believe that at least 10 percent and as much as 30 percent of the ions are transmitted to the Faraday cup when the cage is at ground potential. Under this assumption, Fig. 18 suggests that as much as 30 percent of the produced ions are successfully injected into the RFQ ion guide and cooled.

6 Conclusion

We have built a decelerator system that can successfully decelerate an ISOLDE type ion beam of 60 keV to several tens of eV for injection into an RFQ ion guide. The overall injection efficiency depends on the emittance of the incoming beam but is at least 10 percent for a typical ISOLDE beam, and probably as high as 30 percent for a properly aligned beam. As shown by the work of Taeman Kim, nearly 100 percent of such an injected beam can be captured and cooled for extraction as a beam of emittance less than 1 π·mm·mrad for delivery to experiments. Thus at the expense of at most a factor of ten in intensity, there is a gain, from an initial emittance of 30 π·mm·mrad, of a factor of about 1000 in phase-space density. This should greatly enhance many experiments at ISOLDE involving the detection and observation of rare species of radio-nuclides.

The successful design of such a decelerating system involves careful simulation of possible electrode structures. This was successfully done with a simulation scheme that has a very fast turn-around time so that many possible variations can be investigated in a reasonable time.

Lastly, we have shown that with proper attention to interior surfaces and spacing, it is possible to build a compact deceleration and cooling system that will withstand all the necessary decelerating voltages without electrical breakdown.

References

[1] D. Möhl, "Phase space cooling in storage rings," Physica Scripta **T22**, 21–27 (1988).

[2] Taeman Kim. *Buffer gas cooling of ions in a radio frequency quadrupole ion guide*. Ph. D. thesis, McGill University Montréal (Québec), August 1997. Publication deferred.

[3] B. Jonson, H. L. Ravn, and G. Walter, "ISOLDE PS Booster Facility at CERN: experiments with slow radioactive beams," Nuclear Physics News **3** (2), 5–16 (1993).

[4] G. Bollen *et al.*, "ISOLTRAP: a tandem Penning trap system for accurate on-line mass determination of short-lived isotopes," Nuclear Instruments and Methods in Physics Research A **368**, 675–697 (1996).

[5] H. Raimbault-Hartmann *et al.*, "A cylindrical Penning trap for capture, mass selective cooling, and bunching of radioactive ion beams," Nuclear Instruments and Methods in Physics Research B **126**, 378–382 (1997).

[6] Abdol Mohammad Ghalambor Dezfuli. *Injection, cooling, and extraction of ions from a very large Paul trap*. Ph. D. thesis, McGill University Montréal (Québec), July 1996.

[7] F. M. Penning, Physica (Utrecht) **3**, 873 (1936).

[8] W. Paul, H. P. Reinhard, and U. v. Zahn, Zeitschrift für Physik **152**, 143 (1958).

[9] P. K. Gosh. *Ion traps*. Oxford: Clarendon Press, 1995.

[10] H. G. Dehmelt, Advances in Atomic Physics **3**, 53 (1967).

[11] D. J. Douglas and J. B. French, Journal of the American Society of Mass Spectrometry **3**, 398 (1992).

[12] W. Nernst, Zeitschrift für Physikalische Chemie **2**, 613 (1888).

[13] J. S. Townsend, Philosophical Transactions of the Royal Society of London A **193**, 129 (1899).

[14] J. C. Maxwell, Philosophical Transactions of the Royal Society of London **157**, 49 (1867).

[15] P. Langevin, Annales de Chimie et de Physique **5**, 245 (1905).

[16] A. Einstein, Annalen der Physik (Leipzig) **17**, 549 (1905).

[17] A. Einstein, Zeitschrift für Elektrochemie **14**, 235 (1908).

[18] E. A. Mason and E. W. McDaniel. *Transport Properties of Ions in Gases.* New York: John Wiley and Sons, 1988.

[19] R. B. Moore, "The manipulation of ion beams into and out of electromagnetic traps," Hyperfine Interactions **81**, 45–70 (1993).

[20] William H. Press *et al. Numerical Recipes in C: The Art of Scientific Computing.* Cambridge: Cambridge University Press, 1992.

[21] Peter Varfalvy. *Precision ion optics of axisymmetric electric systems.* M. Sc. thesis, McGill University Montréal (Québec), August 1995.

[22] E. Lamour, "Global efficiency of the cooler (injection part)," report to the CERN/ISOLDE group, December 1998.

[23] E. Lamour (private communication).

[24] A. M. Ghalambor-Dezfuli *et al.*, "A compact 65 keV stable ion gun for radioactive beam experiments," Nuclear Instruments and Methods in Physics Research A **368**, 611–616 (1996).

Appendix A: Technical drawings

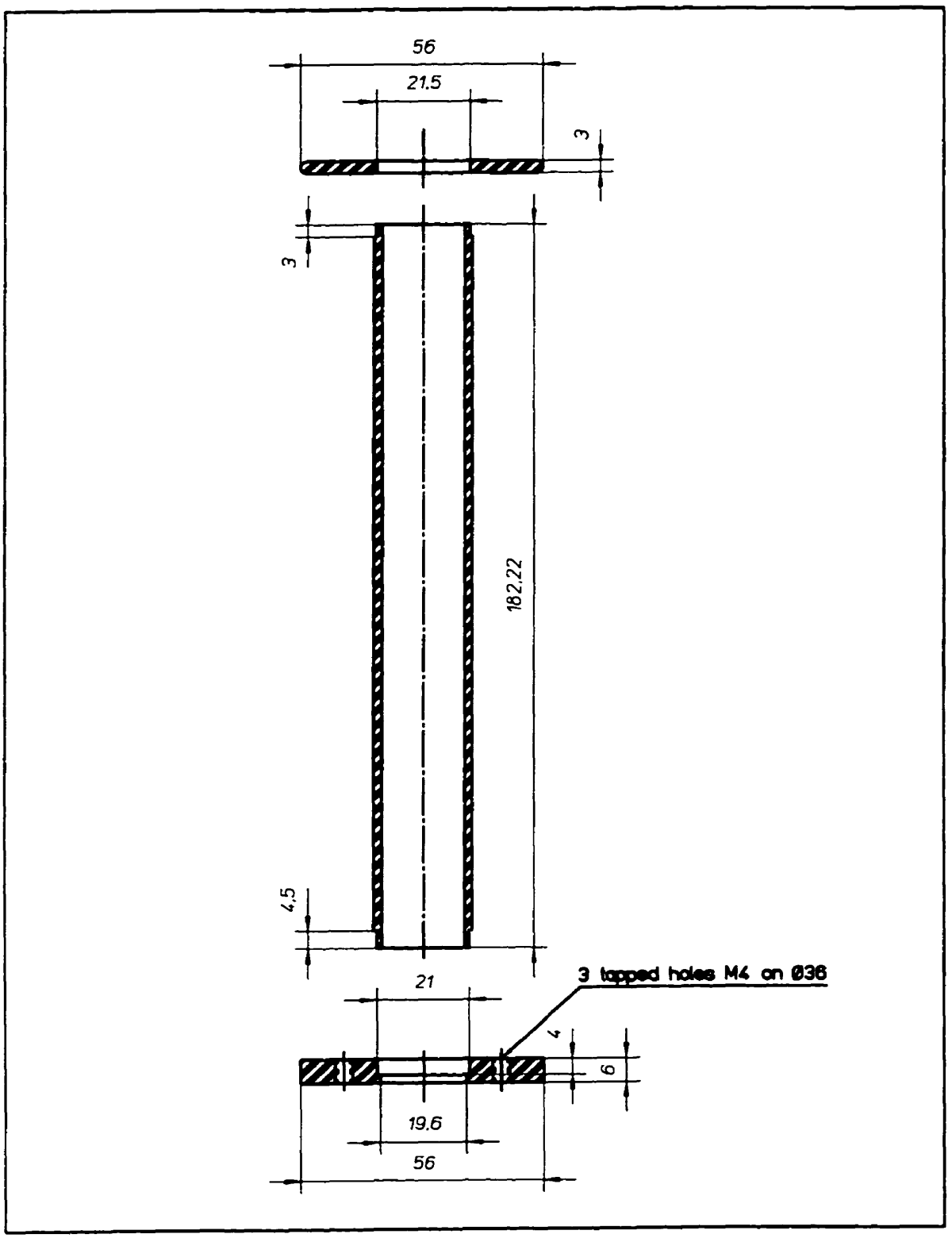

Figure 19: Ground cylinder. Scale 1:1.5.

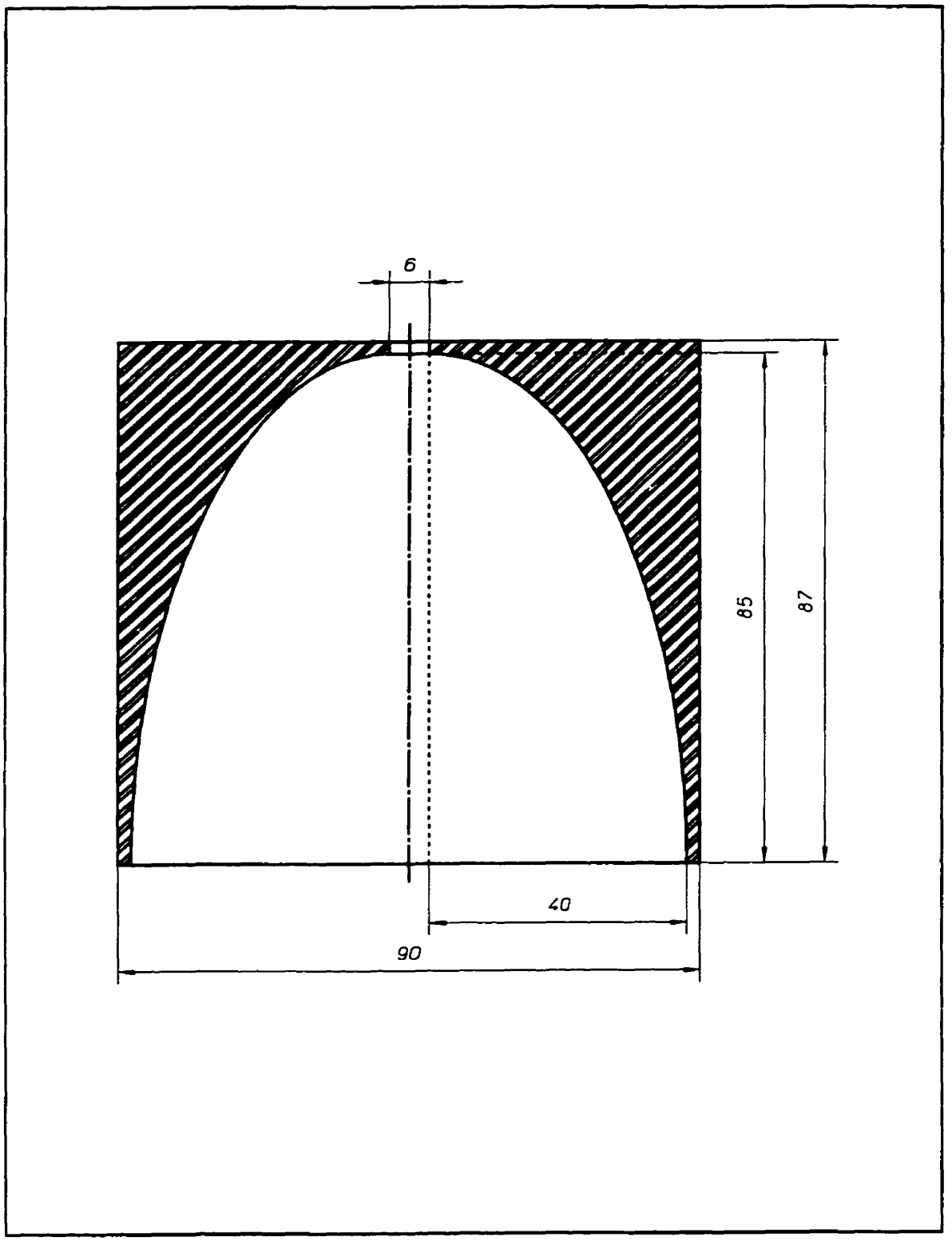

Figure 20: Decelerating electrode. Scale 1:1. The mounting holes for the ceramic spacers on the exit side are not shown

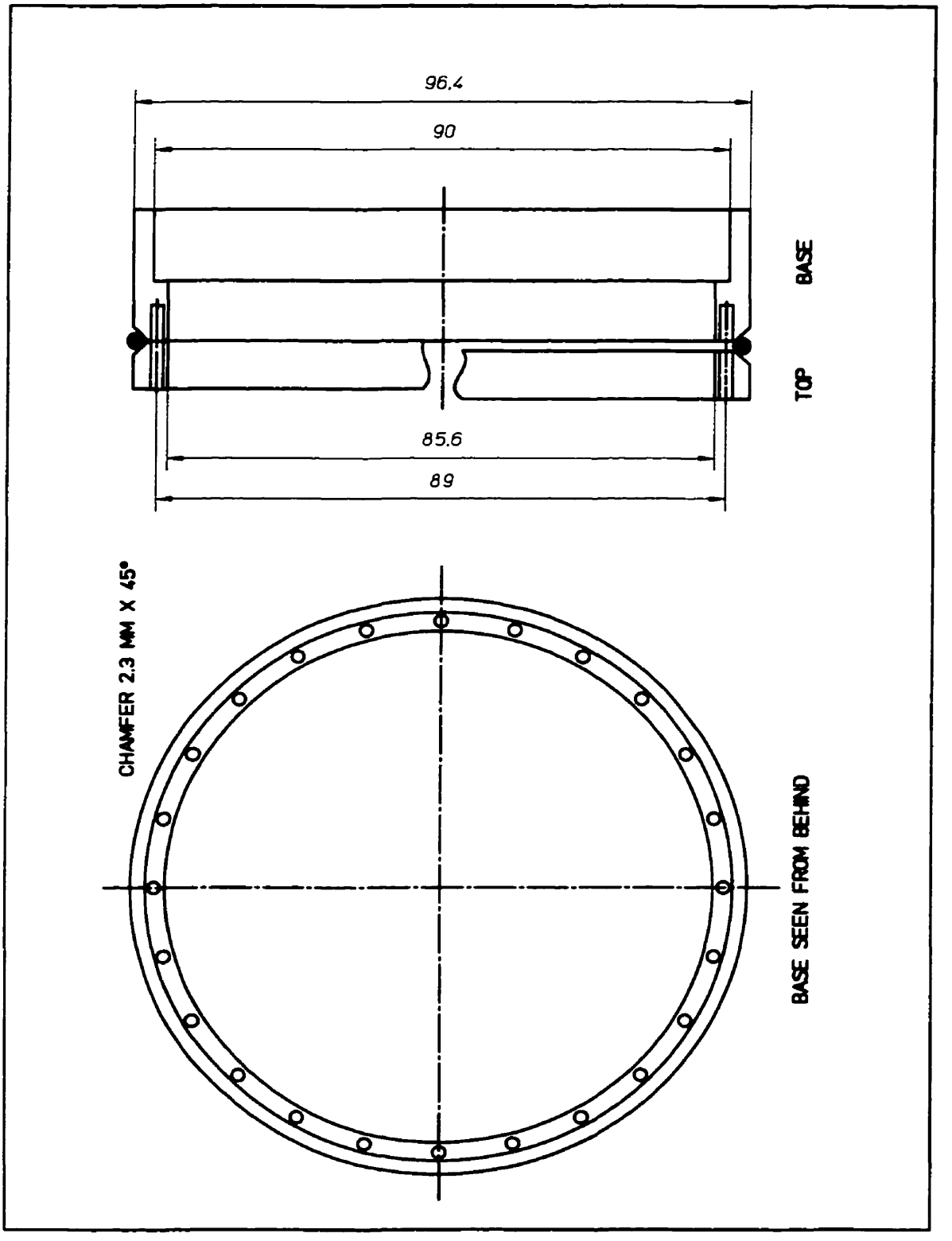

Figure 21: Glass fibre support ring and gas seal for the decelerating electrode. Scale 1:1

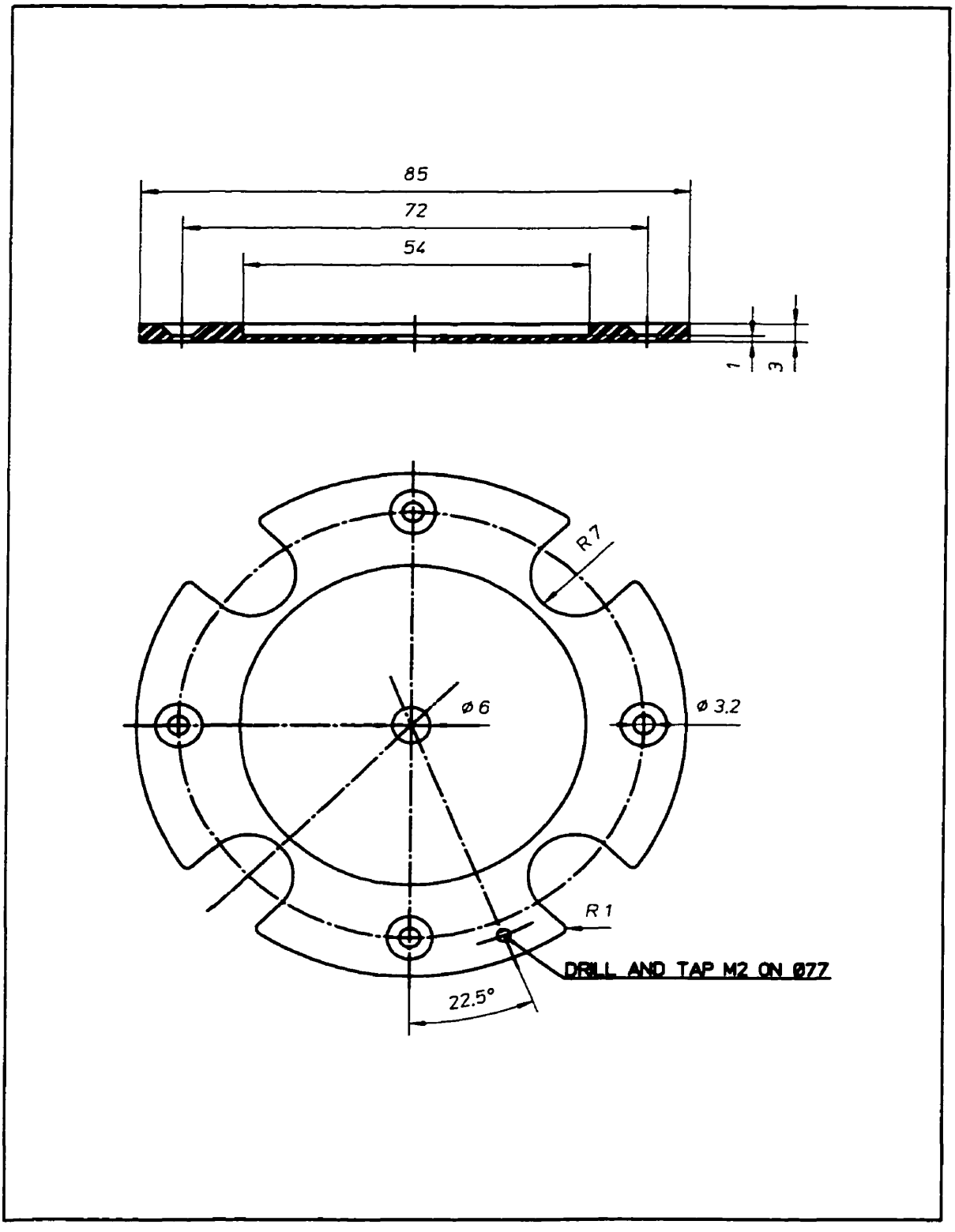

Figure 22: Focusing Electrode. Scale 1:1.

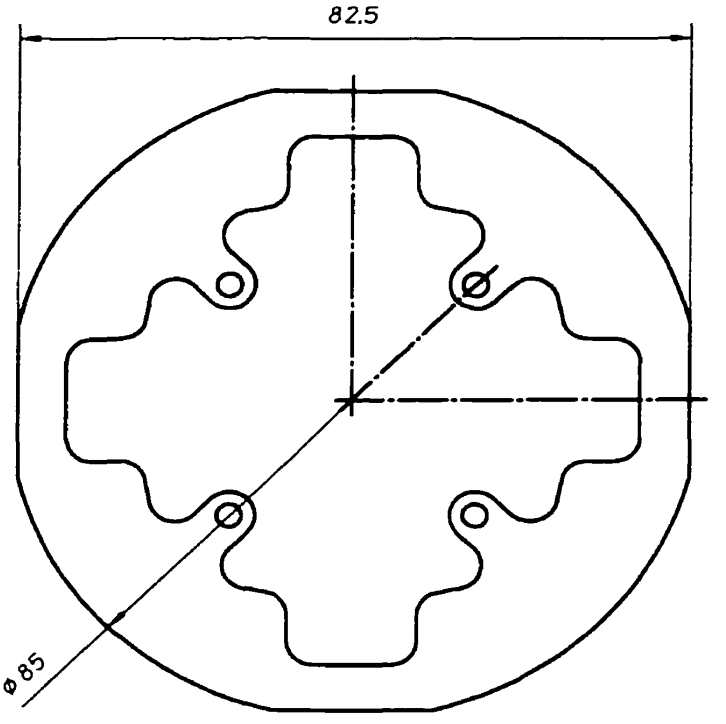

Figure 23: Mounting plate for the ion guide. Scale 1:1. This part was machined on the CNC milling machine and therefore detailed dimensions are not given.

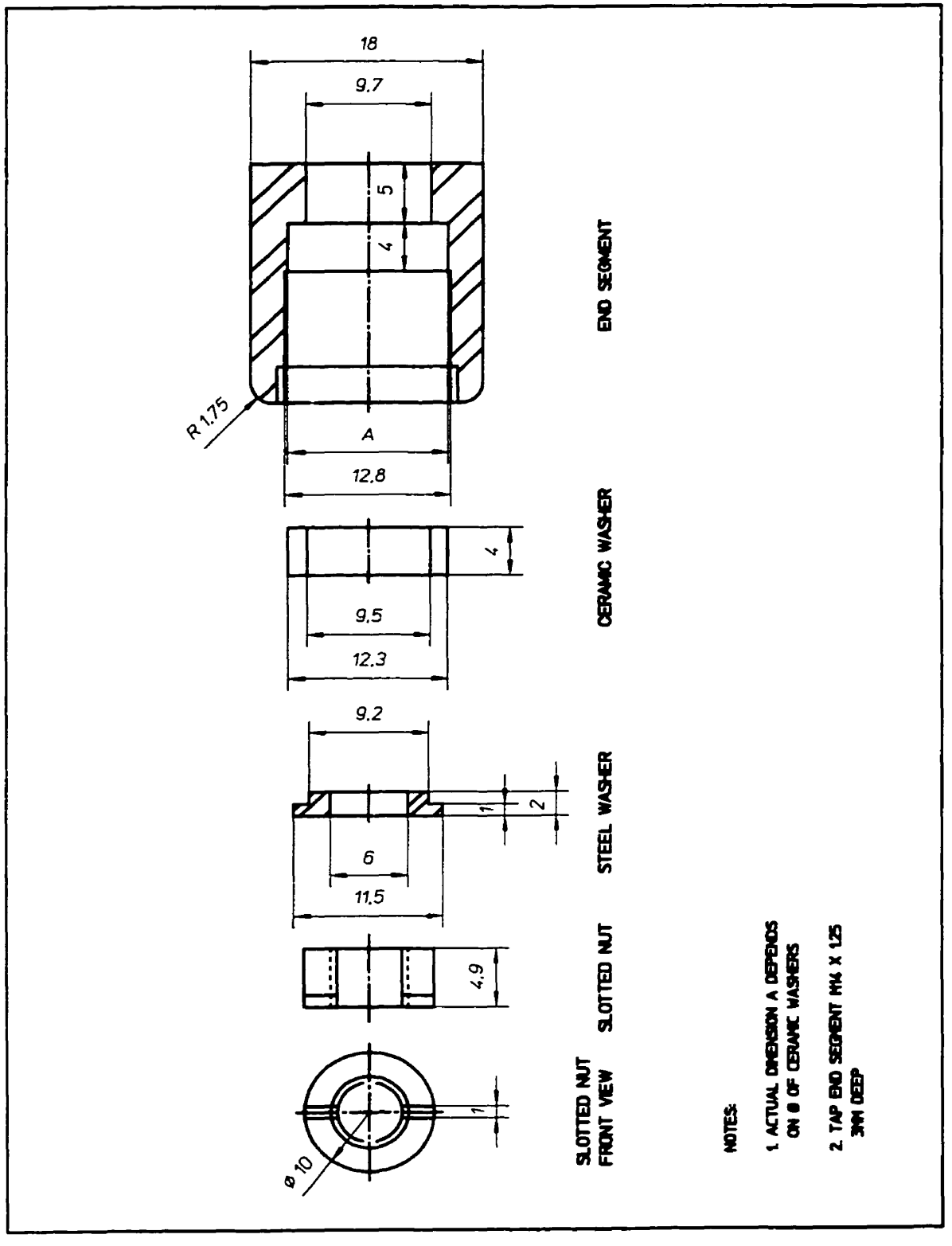

Figure 24: End segment of the ion guide. Scale 2:1.

Appendix B: Photographs

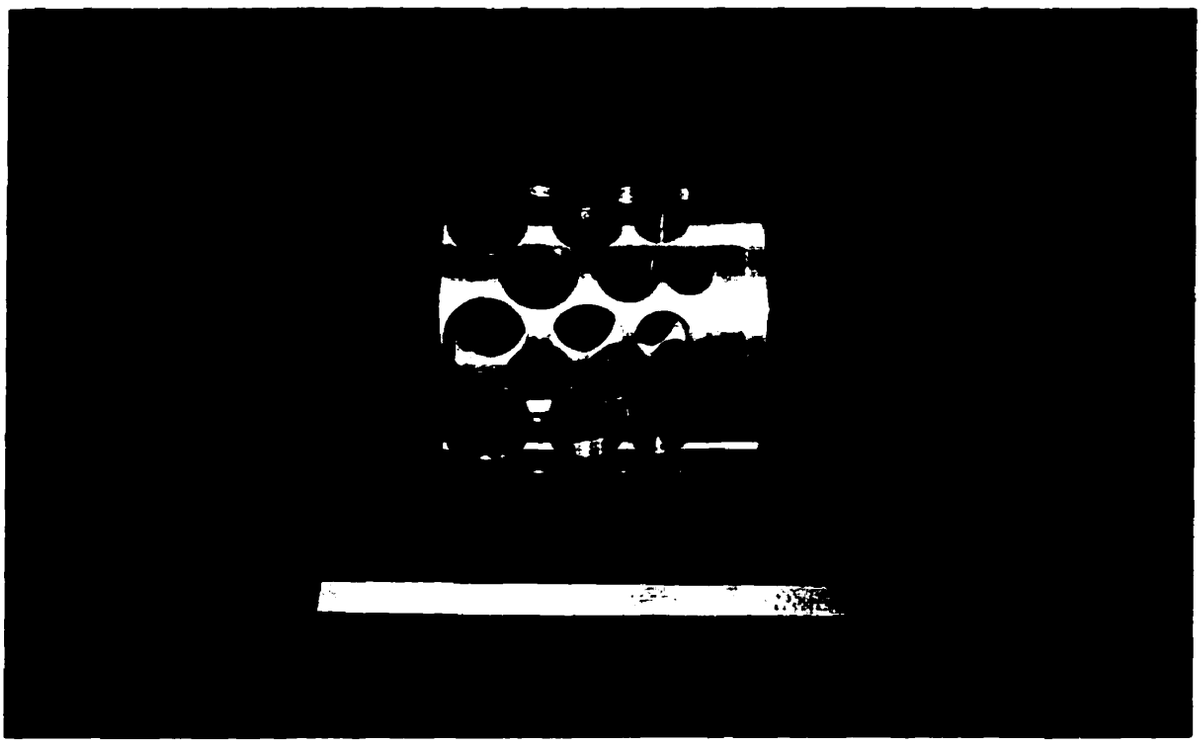

Figure 25: The decelerating electrode. The ruler is 150 mm long.

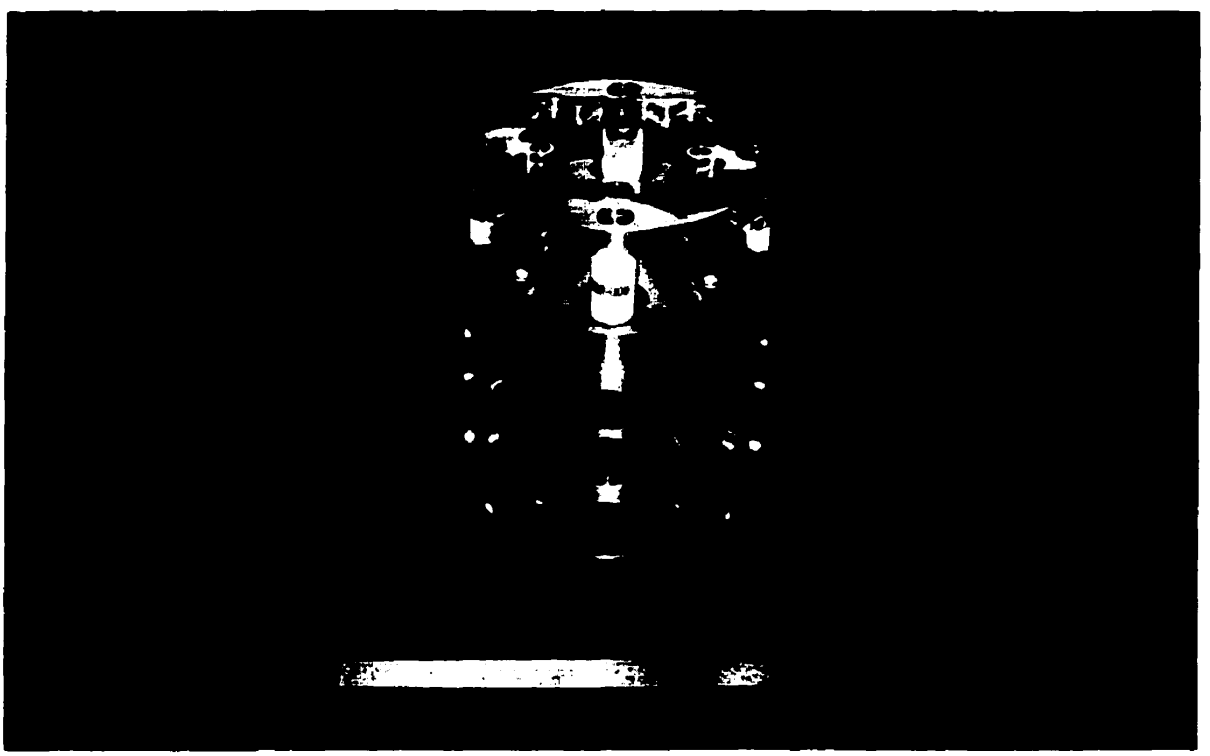

Figure 26: The decelerating electrode, with the focusing electrode and ion guide mounting plates attached. The ruler is 150 mm long.

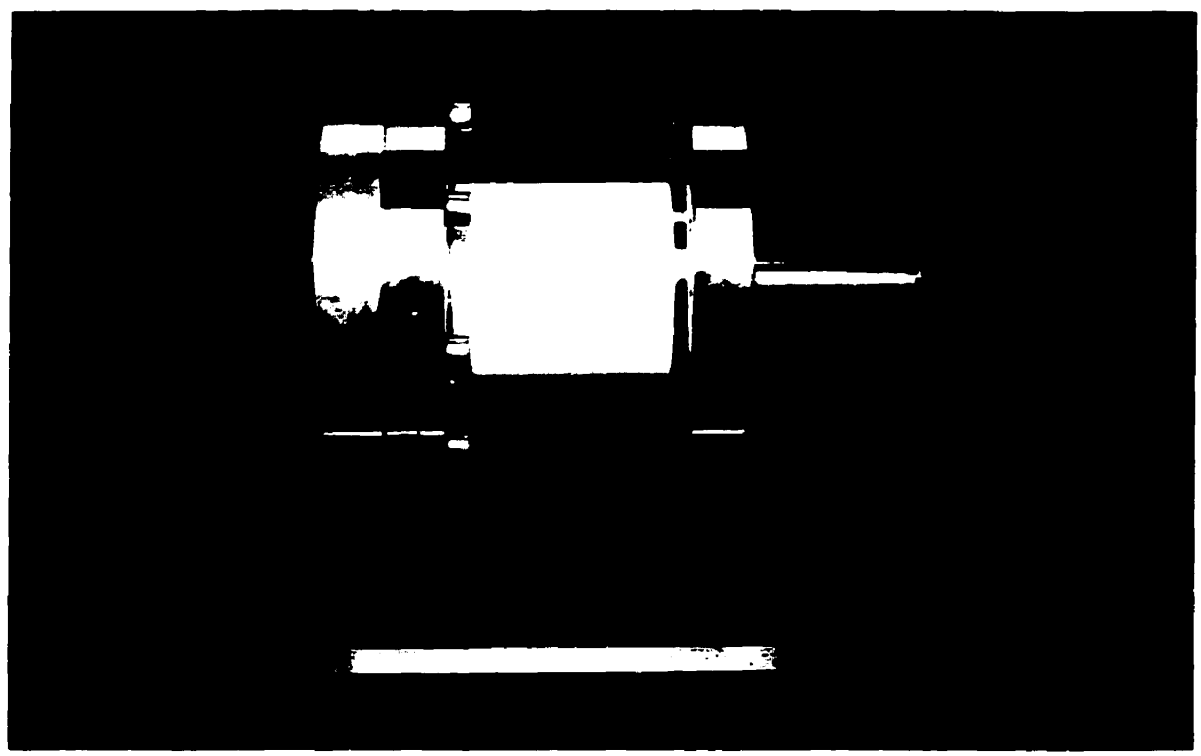

Figure 27: The vacuum break and the inserted ground cylinder. The ruler is 150 mm long.

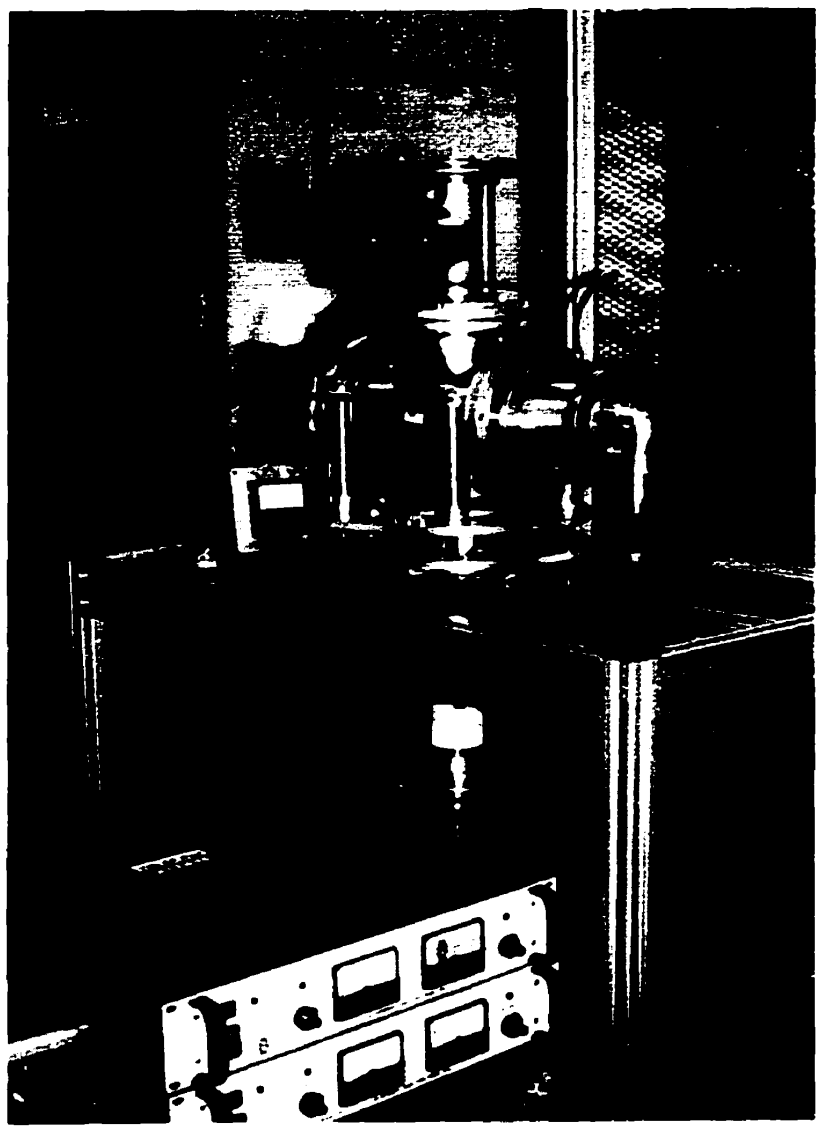

Figure 28: The caesium zeolite ion source.

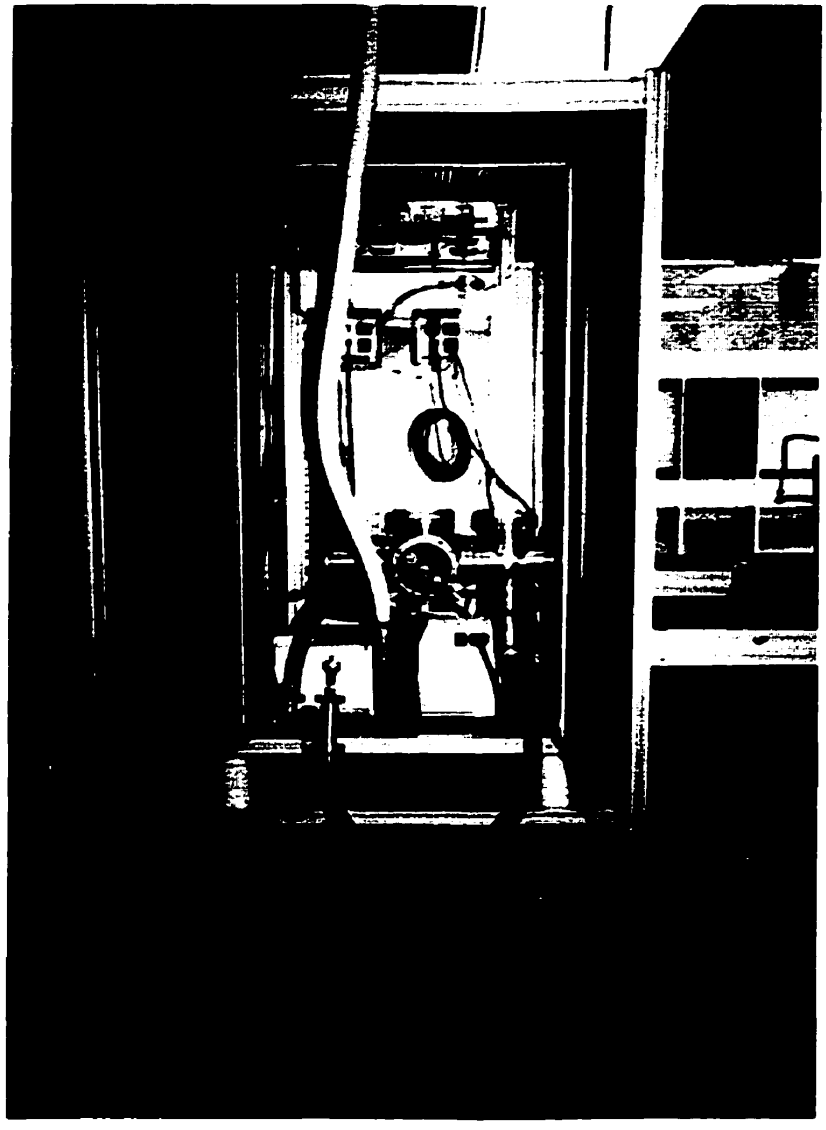

Figure 29: The ground cage and the high-voltage cage. (seen from behind) The vacuum system is already mounted in the high-voltage cage.

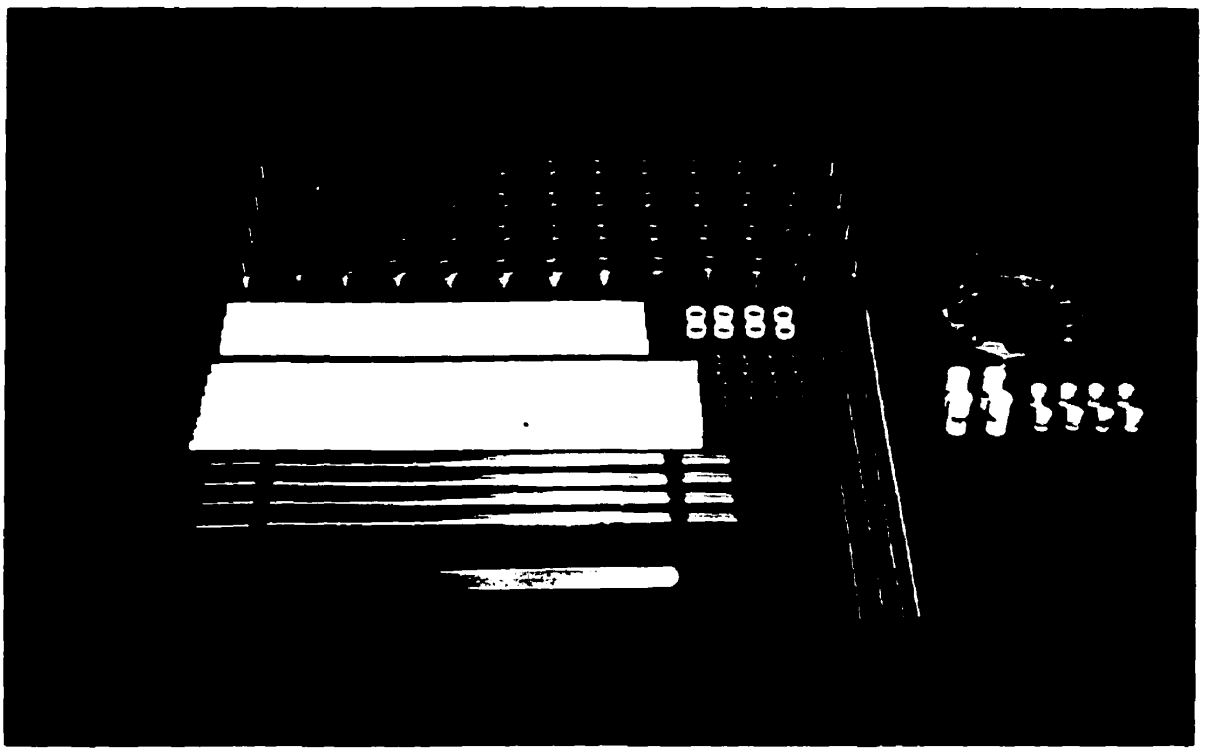

Figure 30: All of the separate parts of the RFQ ion guide. The ruler in the front is 150 mm long.

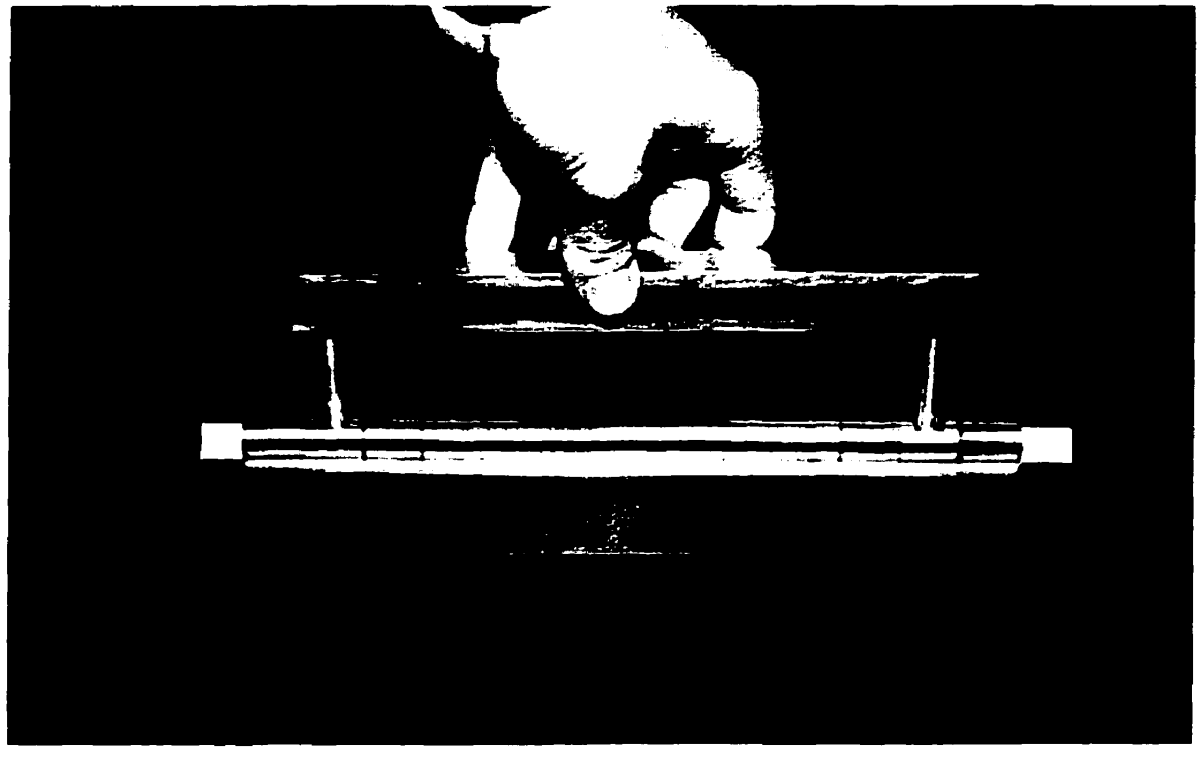

Figure 31: The mounting jig for the RFQ ion guide rods.

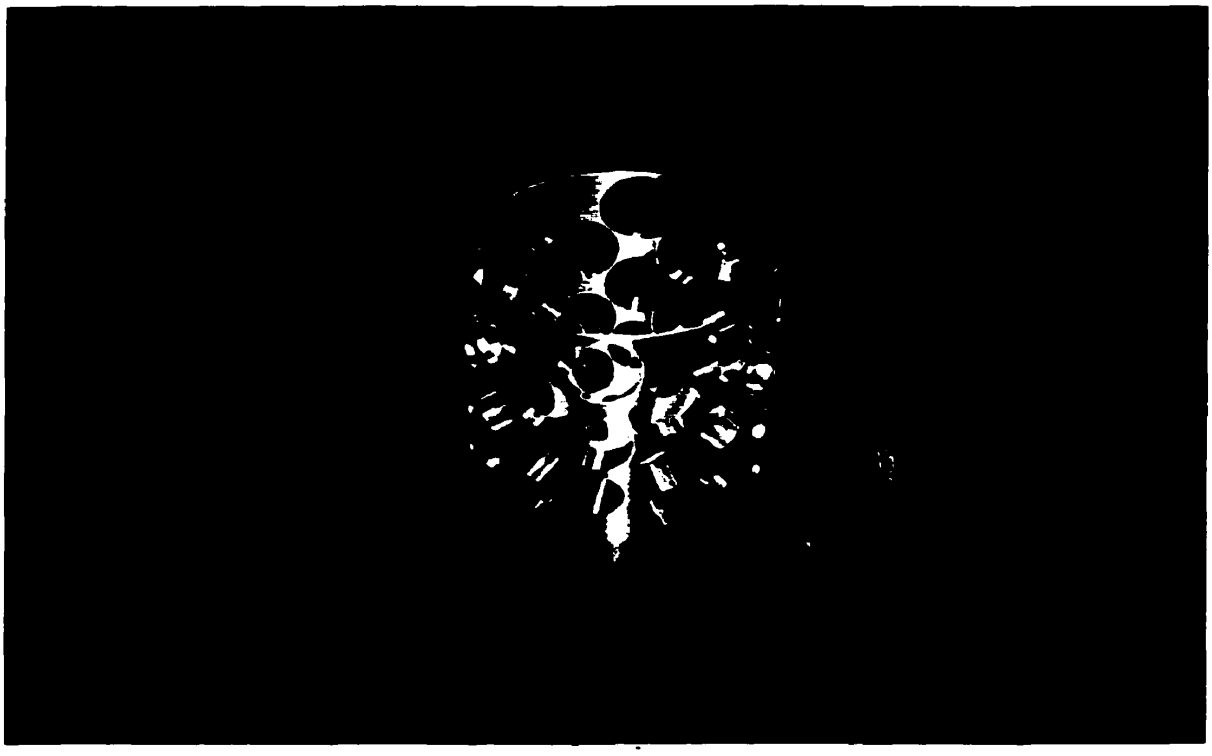

Figure 32: The decelerating electrode, diagonal view.

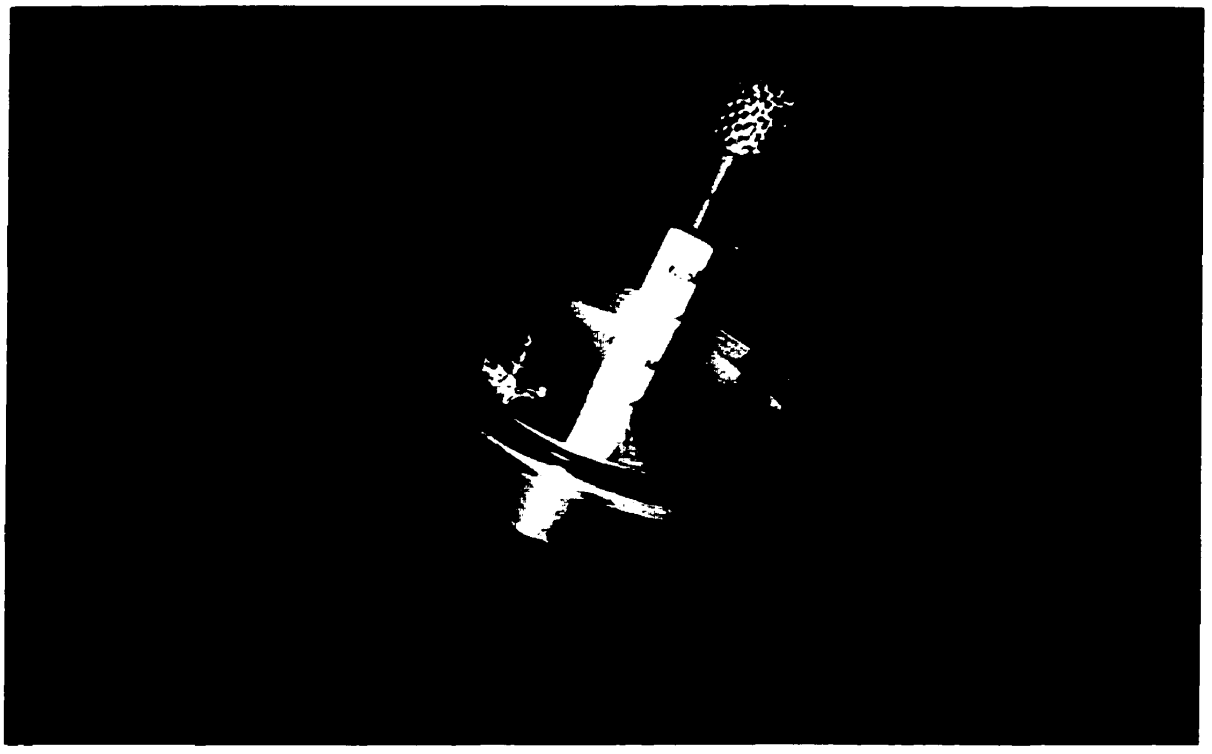

Figure 33: The vacuum flange with the Faraday cup detector mounted on it.

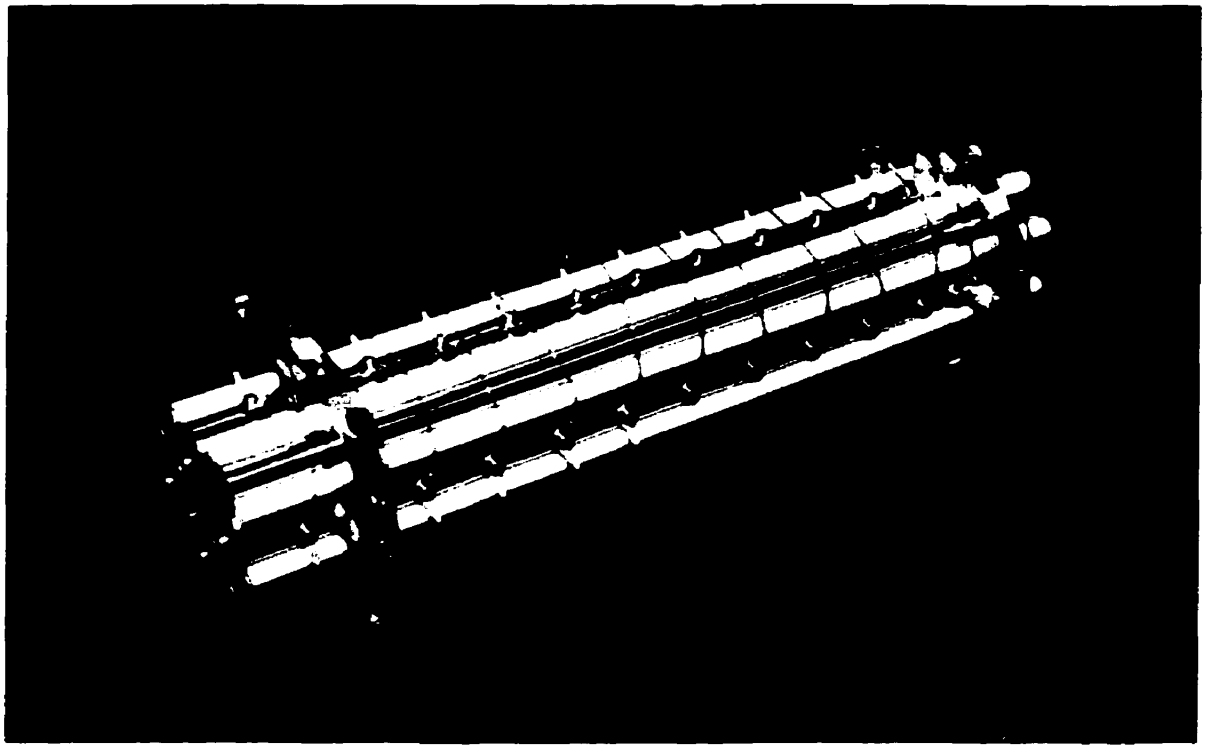

Figure 34: The completely assembled RFQ ion guide.